Paxillin promotes breast tumor collective cell invasion through maintenance of adherens junction integrity

Weiyi Xu, Kyle M. Alpha, Nicholas M. Zehrbach, and Christopher E. Turner*
Department of Cell and Developmental Biology, State University of New York Upstate Medical University, Syracuse, NY 13210

ABSTRACT **Distant organ metastasis is linked to poor prognosis during cancer progression. The expression level of the focal adhesion adapter protein paxillin varies among different human cancers, but its role in tumor progression is unclear. Herein we utilize a newly generated PyMT mammary tumor mouse model with conditional paxillin ablation in breast tumor epithelial cells, combined with in vitro three-dimensional (3D) tumor organoids invasion analysis and 2D calcium switch assays, to assess the roles for paxillin in breast tumor cell invasion. Paxillin had little effect on primary tumor initiation and growth but is critical for the formation of distant lung metastasis. In paxillin-depleted 3D tumor organoids, collective cell invasion was substantially perturbed. The 2D cell culture revealed paxillin-dependent stabilization of adherens junctions (AJ). Mechanistically, paxillin is required for AJ assembly through facilitating E-cadherin endocytosis and recycling and HDAC6-mediated microtubule acetylation. Furthermore, Rho GTPase activity analysis and rescue experiments with a RhoA activator or Rac1 inhibitor suggest paxillin is potentially regulating the E-cadherin-dependent junction integrity and contractility through control of the balance of RhoA and Rac1 activities. Together, these data highlight new roles for paxillin in the regulation of cell–cell adhesion and collective tumor cell migration to promote the formation of distance organ metastases.**

Monitoring Editor
Alpha Yap
University of Queensland

Received: Sep 7, 2021
Revised: Nov 2, 2021
Accepted: Nov 23, 2021

INTRODUCTION

Breast cancer is becoming the most frequent malignancy among women worldwide, but it is curable with early-stage, nonmetastatic diagnosis (Stebbing *et al.*, 2007; Ginsburg *et al.*, 2017). Tumor metastasis is a major cause of cancer-associated mortality in humans (Lambert *et al.*, 2017; Dillekås *et al.*, 2019), involving a series of cellular processes and molecular cues from both the primary tumor and the surrounding tumor microenvironment (Quail and Joyce, 2013; Yates *et al.*, 2017). Invasive cancer cells disseminate from the primary tumors following matrix metalloproteinase-mediated degradation of the basement membrane and then invade into the surrounding stroma, intravasate and extravasate the blood vessels, and finally colonize in distal organs such as the lungs, liver, and brain (Stoletov *et al.*, 2010; van Zijl *et al.*, 2011; Obenauf and Massagué, 2015; Ilina *et al.*, 2018).

Cancer cells can utilize two modes of invasive migration: single cell and collective migration (Cheung and Ewald, 2016; Lambert *et al.*, 2017). In the case of single cell migration, cancer cells undergo epithelia-to-mesenchymal transition (EMT) resulting in loss of cell–cell contact (Ye and Weinberg, 2015). During single cancer cell migration, cells can also exhibit plasticity, transitioning between mesenchymal and amoeboid modes of motility, allowing the tumor cells to remodel the surrounding extracellular matrix (ECM) or squeeze through small gaps in the matrix, respectively, thus leading to efficient individual cell invasion (Friedl *et al.*, 2001; Panková *et al.*, 2010; Bonnans *et al.*, 2014). In contrast, cells using collective migration undergo a partial EMT, with their cell–cell connection remaining intact, and thereby migrate as a cohesive group (Friedl and Gilmour, 2009). While the leader cells in collectively migrating cells use similar

This article was published online ahead of print in MBoC in Press (http://www.molbiolcell.org/cgi/doi/10.1091/mbc.E21-09-0432) on December 1, 2021.

*Address correspondence to: Christopher E. Turner (turnerce@upstate.edu).

Abbreviations used: AJ, adherens junction; BSA, bovine serum albumin; ck14, cytokeratin-14; ECM, cell-ECM; EMT, epithelia-to-mesenchymal transition; FAK, focal adhesion kinase; FBS, fetal bovine serum; FN, fibronectin; GAP, GTPase-activating protein; GEF, guanine-nucleotide exchange factor; H&E, hematoxylin and eosin; KO, knockout; MEM, minimum essential media; MT, microtubule; OCT, optimal cutting temperature; PAK, p21-activated kinase; PBS, phosphate-buffered saline; PFA, paraformaldehyde; WT, wild type.

mechanisms as single cells to polarize, protrude, invade, and adhere to stromal matrix, they are generally more organized and efficient in directed invasion than the individual cells (Friedl and Gilmour, 2009; George *et al.*, 2017; Thuroff *et al.*, 2019).

Collective cell migration requires connection between neighboring cells, coordinating cohesion of cadherin-based adherens junctions (AJs), actomyosin contractility, front-rear polarity, Rho family GTPase activity, as well as cell-ECM interactions (Yamada and Nelson, 2007; Friedl and Wolf, 2008; Vitorino and Meyer, 2008; Cai *et al.*, 2014; Padmanaban *et al.*, 2019). AJs are highly dynamic, with E-cadherin being removed from the plasma membrane by clathrin-dependent and -independent endocytosis and sorted back to the cell surface through the *trans*-Golgi network and the Rab11 positive recycling endosome (Le *et al.*, 1999; Paterson *et al.*, 2003; Brüser and Bogdan, 2017). The equilibrium between accumulation and turnover of the cadherin complex at the cell surface allows epithelial sheets to remodel without losing their cell–cell contact (Le *et al.*, 1999; Kametani and Tacheichi, 2007; Pinheiro and Bellaiche, 2018).

Cohesive groups of tumor cells establish a front-to-rear polarity axis through cytoskeletal rearrangement and modulation of Rho GTPase activity (Nobes and Hall, 1999; Farooqui and Fenteany, 2005). Activation of the Rho GTPases, Cdc42, and Rac1 promotes actin reorganization to provide forward membrane extension in the leader cells, whereas RhoA is activated at the cell rear to generate actomyosin-dependent contraction forces that drag the following cells forward (Farooqui and Fenteany, 2005; Yamada and Nelson, 2007). Additionally, cell–ECM signaling in the leader cells, involving β1–integrin-dependent activation of the focal adhesion kinase (FAK) triggers downstream signaling resulting in remodeling and alignment of the ECM (Bonnans *et al.*, 2014; Ilina *et al.*, 2020) to further promote directed collective migration (Takahashi *et al.*, 2003; Keely, 2011).

Paxillin (Turner *et al.*, 1990) is a scaffold/adapter protein that localizes to sites of cell–ECM interaction, called focal adhesions, and plays various critical roles in the ECM-integrin signaling network (Turner, 2000; Brown and Turner, 2004; Deakin and Turner, 2008; Scheswohl *et al.*, 2008; López-Colomé *et al.*, 2017; Alpha *et al.*, 2020). In cancer cells activated by ECM signals, paxillin also recruits GTPase-activating proteins (GAPs) and guanine-nucleotide exchange factors (GEFs) and Rho GTPase effector proteins to focal adhesion sites to coordinate the spatio-temporal activity of Rho GTPases and downstream signaling (Turner *et al.*, 1999; Schaller, 2001; Brown *et al.*, 2002; LaLonde *et al.*, 2006; Deakin *et al.*, 2012; López-Colomé *et al.*, 2017). Furthermore, more recent studies have shown that paxillin regulates Golgi positioning and integrity and front-rear polarity initiation through HDAC6-dependent microtubule (MT) deacetylation, thereby regulating directional anterograde vesicle trafficking to further modulate single cell movement (Deakin and Turner, 2014; Dubois *et al.*, 2017).

Large-scale transcriptomic or gene specific analyses in different patient samples have revealed that paxillin is differentially expressed in cancers, including but not limited to lung cancer, colorectal carcinoma, osteosarcoma, and breast cancer (Bhattacharjee *et al.*, 2001; Zhao *et al.*, 2004; Azuma *et al.*, 2005; Farmer *et al.*, 2005; Radvanyi *et al.*, 2005; Turashvili *et al.*, 2007; Kanteti *et al.*, 2009; Yang *et al.*, 2010). In most cases, paxillin is shown to be down-regulated in breast cancer; however, in an earlier study, paxillin was shown to be up-regulated in HER family member positive breast cancer biopsies (Vadlamudi *et al.*, 1999), and a more acute clinical study showed paxillin correlates with *HER2* amplification and may influence the clinical response to chemotherapy in breast cancer patients (Short *et al.*, 2007). The up- or down-regulation for paxillin in breast cancer patients suggests that a role for paxillin as either an oncogene or a tumor suppressor may be based on tumor type, stage, and the surrounding environment. Therefore, precisely how paxillin may regulate breast tumor progression still needs to be described.

Herein we utilized a newly developed paxillin conditional knockout (KO) mouse (Rashid *et al.*, 2017; Xu *et al.*, 2019), in combination with the MMTV-PyMT breast tumor mouse (Lin *et al.*, 2003) that is comparable to human ER, PR negative, HER2 positive breast cancer to assess paxillin function in tumor progression. These in vivo studies, combined with three-dimensional (3D) tumor organoid culture and 2D primary cell culture systems, revealed a previously unappreciated role for paxillin in the regulation of AJ cell–cell adhesion integrity necessary for collective tumor cell migration and metastasis.

RESULTS

Paxillin facilitates lung metastasis in mouse breast tumor progression

We have previously reported that paxillin is required for normal mouse mammary gland morphogenesis and development in a mammary epithelial cell-specific MMTV-cre-mediated paxillin conditional KO mouse (Xu *et al.*, 2019). Herein, this mouse line was bred with the MMTV-PyMT tumor mouse model in order to evaluate paxillin function in breast tumor progression. To determine whether the loss of paxillin expression in the mammary epithelial cells affects tumor onset and tumor growth, we monitored the mice weekly after 6 wk postnatally. We observed that in the paxillin KO mice the total and primary tumor volume was slightly reduced and the tumor latency was marginally delayed, as compared with wild-type (WT) control mice, but the differences were not statistically significant (Figure 1, A and C, and Supplemental Figure S1A). Western blot analysis of whole tumor lysates and the isolated tumor cell lysates confirmed that paxillin is depleted in the KO mice tumors (Figure 1B). Immunofluorescence staining of tumor sections revealed that paxillin is selectively depleted in tumor cells but not from the surrounding stroma cells (Figure 1D).

Since paxillin did not significantly affect tumor growth, as shown by ki67 staining (Supplemental Figure S1, B and C), which is consistent with the study showing that in normal mouse mammary gland the proliferation and apoptosis rates are not altered by paxillin KO (Xu *et al.*, 2019), we assessed whether distant metastasis is impacted by paxillin expression. Hematoxylin and eosin (H&E) staining of lung sections and analysis of the surface of the whole lungs from the PyMT tumor mice revealed that the paxillin KO lungs have fewer lung metastases, as compared with paxillin WT lungs (Figure 1, E-G). Taken together, these data suggest that paxillin plays a key role in malignant tumor invasion and dissemination.

Paxillin depletion leads to reduced invasion in primary breast tumors

For the primary tumor cells to colonize and form metastatic tumors in distant organs, the cells must undergo local invasion, intravasation, dissemination, and extravasation (Lambert *et al.*, 2017). Therefore we first determined whether the reduction in lung metastasis in the paxillin KO tumor mice is associated with attenuated tumor cell invasion. In normal mammary glands, only the myoepithelial cells express the basal epithelial gene—cytokeratin-14 (ck14). However, in highly invasive carcinomas, the tumor cells also express ck14. Thus, ck14 expression serves as a useful marker for tumor invasiveness (Lichtner *et al.*, 1991; Cheung *et al.*, 2013). To determine whether paxillin KO tumors are less invasive, tumor sections were immunostained for ck14 and the tumor cell marker EpCAM. Interestingly, at the early hyperplasia or adenoma stage, the myoepithelial layer is lost with an increasing number of ck14 positive tumor cells in the paxillin WT

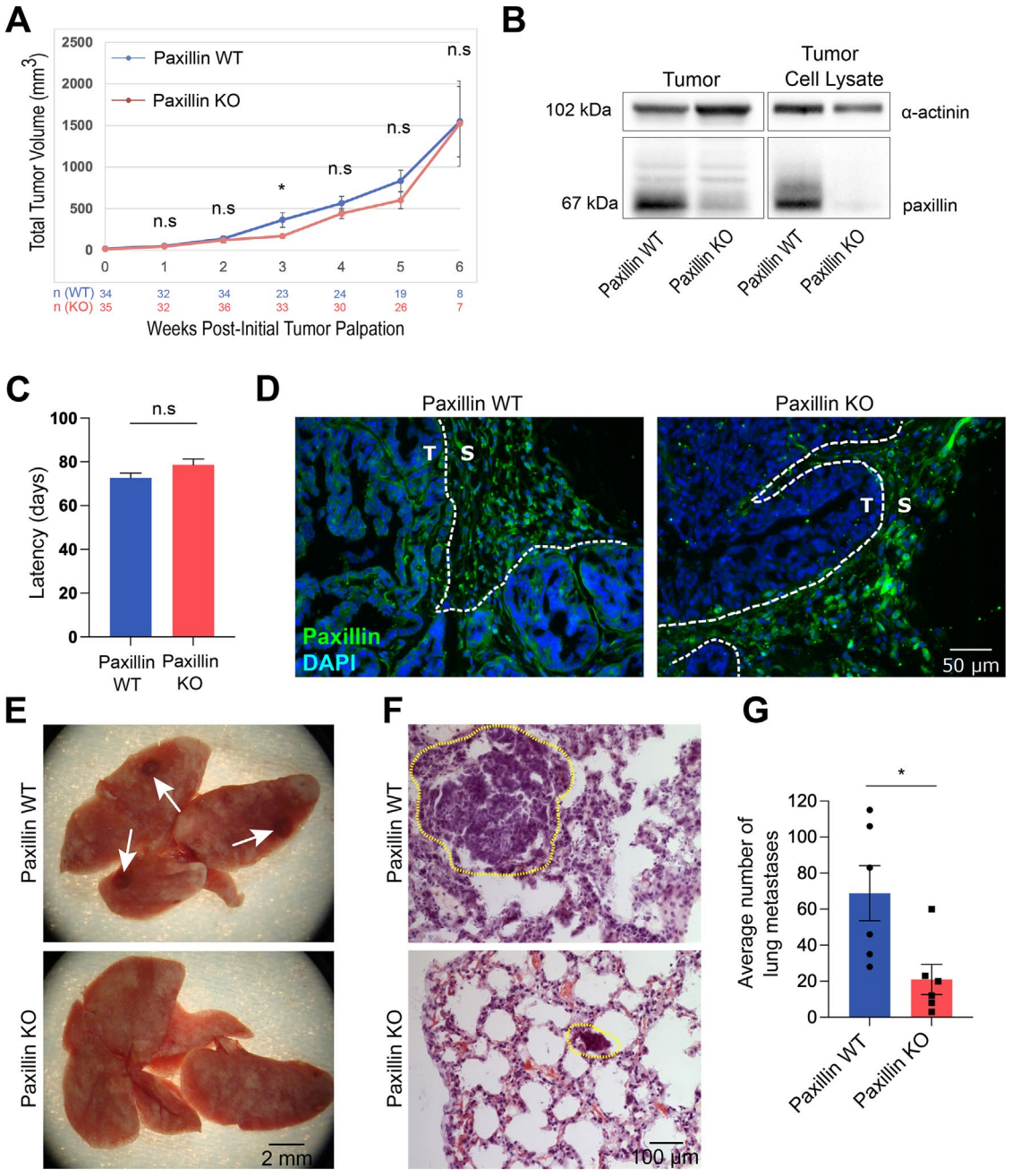

FIGURE 1: Paxillin KO breast tumor mouse develops fewer lung metastases. (A) Paxillin expression does not significantly affect total tumor size; *n* = number of animals. (B) Western blot showing paxillin is absent in KO tumor and isolated tumor cell lysates. (C) Paxillin does not affect tumor latency; *n* (animals) (paxillin WT) = 39, *n* (paxillin KO) = 36. (D) Paxillin is depleted only in KO tumor cells and not stroma cells as visualized by immunofluorescence staining of tumor sections. T, tumor; S, stroma. (E) Whole lungs. White arrows show surface metastases. (F) H&E staining of lung sections. Lung metastases are highlighted with dashed circles. (G) Quantification of total number of lung metastases; *n* = 6 animals per genotype. A Student's *t* test was performed for statistical analysis. Data represent mean ± SEM *< 0.05.

tumor mice, whereas in the paxillin KO tumor mice, the myoepithelial layer remains intact and encapsulates the ck14 negative tumor cells (Figure 2, A–C). Moreover, as the paxillin WT tumors progressed to the carcinoma stage, ck14 positive cells clustered together in the bulk tumor and invaded into the stroma as small groups (Figure 2C). Compared with the WT control, the paxillin KO tumors had fewer ck14 positive tumor cells in both the bulk tumor and stroma (Figure 2, A–D), suggesting that paxillin expression in the tumor cells is critical for a more invasive phenotype in the primary tumor.

Recent studies have shown that in highly invasive breast cancer, cells accomplish collective invasion through maintaining cell–cell contacts (Friedl and Gilmour, 2009; Cheung and Ewald, 2016; Padmanaban *et al.*, 2019). Accordingly, we stained the tumor sections for the AJ marker, E-cadherin (Figure 2E). At the tumor-stroma border, groups of paxillin WT tumor cells, with E-cadherin enrichment at cell–cell boundaries, were observed collectively invading into the stroma (Figure 2E, top). However, in the paxillin KO tumor, very few tumor cells invaded into stroma, and the ones that invaded

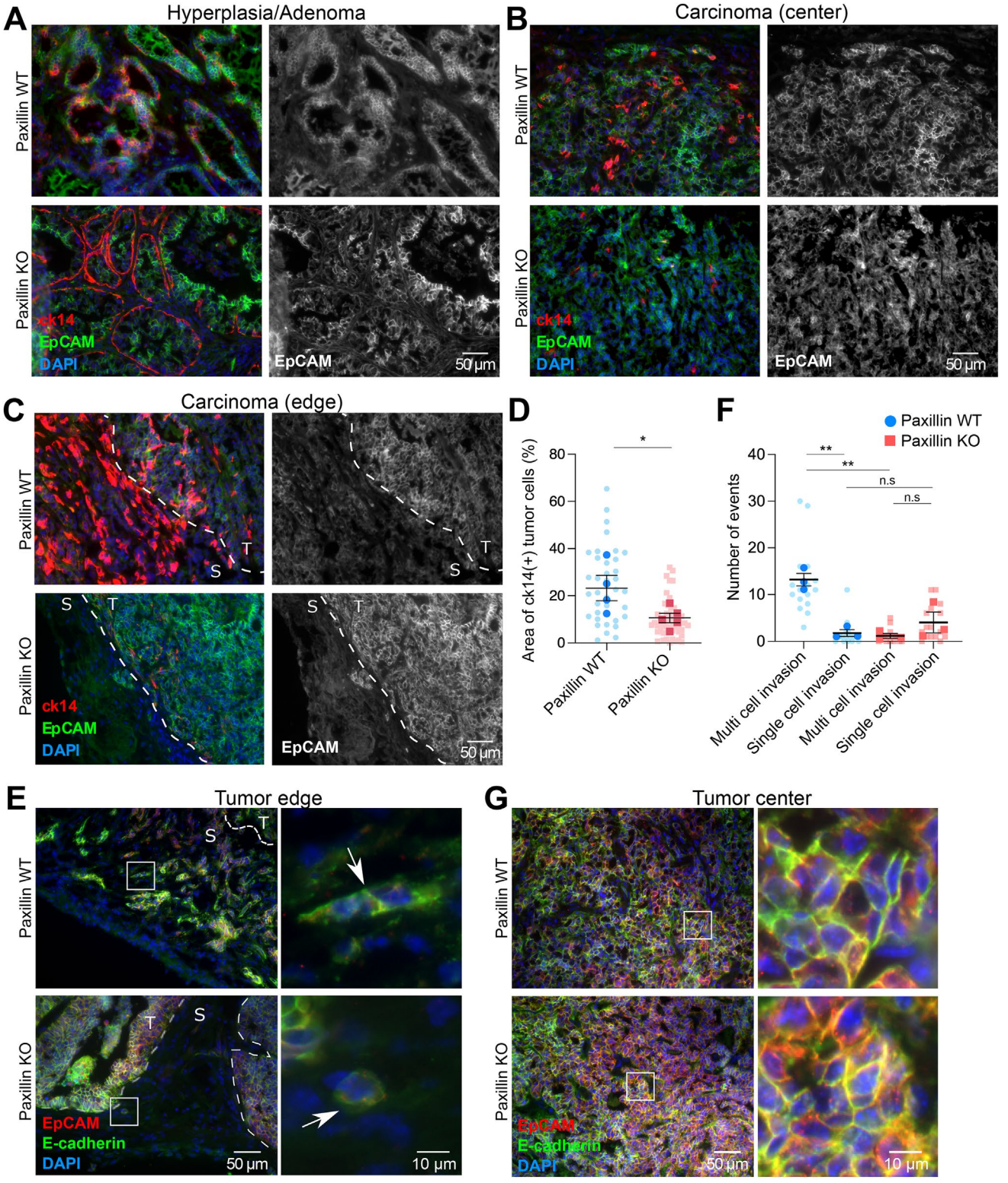

FIGURE 2: Paxillin KO primary tumors are less invasive. Representative tumor sections from (A) early stage (hyperplasia or adenoma) tumors and the center (B) and the edge (C) of late stage (carcinoma) tumors stained for the tumor marker EpCAM and invasiveness marker ck14. The gray scale images show EpCAM-positive tumor cells. T, tumor; S, stroma. (D) Quantification of area of ck14 positive tumor cells; *n* (paxillin WT) = 4 animals, *n* (paxillin KO) = 5 animals. Each dot represents one image. (E) Paxillin WT tumor cells invade into the stroma collectively at the tumor edge (arrow top); few paxillin KO tumor cells invade into the stroma, and these were individual cells (arrow bottom). (F) Quantification of multicell, collective invasion and single cell invasion. Each string/group of tumor cells or a single cell in the stroma was counted as an event; *n* = 3 animals per genotype. (G) E-cadherin-mediated cell–cell junction organization is not affected in the tumor center of either paxillin WT or paxillin KO animals. A Student's *t* test was performed for statistical analysis. Data represent mean ± SEM *< 0.05, **< 0.01.

were primarily single cells (Figure 2E, bottom). Quantification of multicell invasion versus single cell invasion, based on EpCAM staining or E-cadherin staining, revealed that paxillin KO tumors exhibited significantly reduced collective tumor cell invasion along with a small increase in single cell invasion that was not statistically significant (Figure 2F). Of note, at the tumor center, both paxillin WT and KO tumor cells exhibited robust cell–cell AJs (Figure 2G). Together these data suggest that paxillin is required for collective invasion in the primary tumor and maintenance of cell AJs at a nonsteady state at the tumor/stroma boundary. Interestingly, although paxillin does not localize to AJs either in vivo or in cultured epithelial cells (Turner *et al.*, 1991; Xu *et al.*, 2019), the normal mammary gland also needs paxillin to form mature AJs during tissue morphogenesis (Supplemental Figure S2).

Tumor organoids lacking paxillin are less invasive in 3D collagen culture

To reduce the potential influence of the surrounding tumor microenvironment and other types of stromal cells, such as fibroblasts and macrophages (Friedl and Alexander, 2011; De Palma *et al.*, 2017; Hamidi and Ivaska, 2018), and to quantitatively evaluate the cell autonomous role of paxillin in tumor invasiveness and AJ integrity, we utilized 3D tumor organoid cultures to recapitulate tumor progression ex vivo (Nguyen-Ngoc *et al.*, 2015). Tumor epithelial cells were isolated from the paxillin WT and KO animals and then cultured in 3D collagen gels (Padmanaban *et al.*, 2020). Consistent with the observed reduction in invasion in the primary tumor, organoids from the paxillin KO animals exhibited a reduced capacity to invade collectively into the collagen gel, as evaluated by the degree of circularity of the organoids and by counting the number of multicell protrusions (Figure 3, A–D; Supplemental Figure S3A). In contrast, the tumor cells in paxillin WT organoids invaded into the collagen gel as multiple cohesive groups, with their AJs, as visualized by staining for E-cadherin, being well-maintained. Furthermore, while paxillin and vinculin localization was mostly cytosolic in the paxillin WT tumor organoids, they were also enriched at potential 3D matrix adhesion sites in the leader cells (Supplemental Figure S3B). Additionally, phase-contrast time-lapse movies revealed that, in contrast to the collective invasion of the paxillin WT tumor organoids, the paxillin KO tumor cells exhibited only single cell invasion into the surrounding matrix (Figure 3, B and E, and Supplemental Figure S3C; Supplemental Movies S1 and S2). Interestingly, a fraction of the paxillin KO single cells had an elongated morphology in 3D invasion (Figure 3C asterisk), comparable to MDA-MB-231 breast cancer cells following paxillin RNAi-mediated knockdown (Deakin and Turner, 2011). Together these data identify a role for paxillin in the organization of E-cadherin-rich AJs to facilitate collective tumor invasion.

Paxillin is required for tumor cell collective migration in 2D culture

The in vivo mouse model and 3D tumor organoid studies demonstrate that paxillin is required for collective invasion and AJ maintenance. To begin to explore the underlying mechanism, we utilized a modified 2D wound healing assay. Cells were seeded into a silicon chamber to form a compact monolayer, and then the chamber was removed and cells were allowed to move into the ECM-containing void. Phase-contrast time-lapse movies were generated to record the motility of the cells. At the leading edge, the paxillin KO cells were more separated from each other and exhibited increased random movement as compared with the paxillin WT cells that remained more cohesive (Figure 4A; Supplemental Movies S3 and S4). Quantification of key motility parameters revealed that the paxillin KO cells exhibited reduced directionality and migration area (Figure 4, B and C).

Paxillin is required for AJ organization

To further assess AJ organization in the paxillin KO cells, the cells were allowed to migrate for 8 h, then stained for E-cadherin (Figure 4D; Supplemental Figure S4, A and B). At the migration leading edge, the E-cadherin and to a lesser extent vinculin staining of AJs in paxillin WT cells demonstrated a linear distribution and the F-actin aligned in parallel with the AJ at the cell's periphery (Figure 4D, upper right, and Supplemental Figure S4B), typical of mature AJs (Efimova and Svitkina, 2018). In contrast, the paxillin KO cells exhibited a more punctate E-cadherin and vinculin staining at the cell–cell interface, with the F-actin aligning perpendicular to the cell interface (Figure 4D, lower right, and Supplemental Figure S4B), which is more typical of disorganized AJs, either bridge AJs or retraction fibers (Efimova and Svitkina, 2018). Conversely, vinculin-containing cell–ECM focal adhesions or vinculin expression remained largely unperturbed in the paxillin KO tumor cells (Figure 4D and Supplemental Figure S4, C and D). Further quantification, using an AJ index (see *Materials and Methods* for details), indicated that the paxillin KO cells at the leading edge displayed a significant reduction in the number of mature AJs as compared with the paxillin WT cells (Figure 4E). However, interestingly, the AJs were still largely retained in paxillin KO cells at the center of the monolayer (Figure 4D and Supplemental Figure S4A), as observed in the primary tumor. Similar defects in AJ junction organization were observed when the paxillin KO cells were seeded onto fibronectin (FN)-coated 2D substrates to allow for the formation of small cell colonies (10–70 cells) and stained for E-cadherin, p120ctn, and F-actin (Supplemental Figure S5).

AJs function to connect cells and maintain cell architecture and morphology via the balancing of actomyosin-mediated contractile forces between neighboring cells (Carthew, 2005; Iyer *et al.*, 2019; Greig and Bulgakova, 2020; Gupta *et al.*, 2021). Therefore, cell shape and area were also assessed using Imaris analysis tools (Supplemental Figure S6A). The paxillin KO cells, when plated in small islands, exhibited a higher aspect ratio (Supplemental Figure S6B), as well as increased average and range of cell area, as compared with the paxillin WT cells (Supplemental Figure S6, C and D), consistent with disruption of cell contractility and AJ function following paxillin depletion.

Paxillin-dependent AJ organization is established in part through regulation of E-cadherin vesicle trafficking

To determine whether paxillin is required for the formation of new AJs, the 2D-cultured cell colonies were subjected to a calcium switch assay involving treatment with EGTA to first dissociate all the calcium-dependent AJs and then recovery by replacing the cells back into normal calcium-replete culture media. Following calcium restoration, the cells were analyzed using phase-contrast time-lapse movies to monitor AJ reformation (Supplemental Movies S5–S8). Paxillin WT cells reformed their AJs using a typical "zipperlike" mechanism (Supplemental Movie S7) (Greaves, 2000), whereas the paxillin KO cells failed to form stable AJs over the 6 h duration of the movie (Supplemental Movie S6). Instead, on initial cell–cell contact, the paxillin KO cells frequently pulled away from each (Supplemental Movie S8, arrow). In addition, the paxillin WT and KO cells were fixed at different time points, following calcium addition, to reveal the time course of AJ recovery (Figure 5A). WT cells readily formed new AJs within 120 min. However, consistent with the staining of unperturbed cells (Supplemental Figure S5A), paxillin KO cells, although able to respread on the substrate and form vinculin-rich

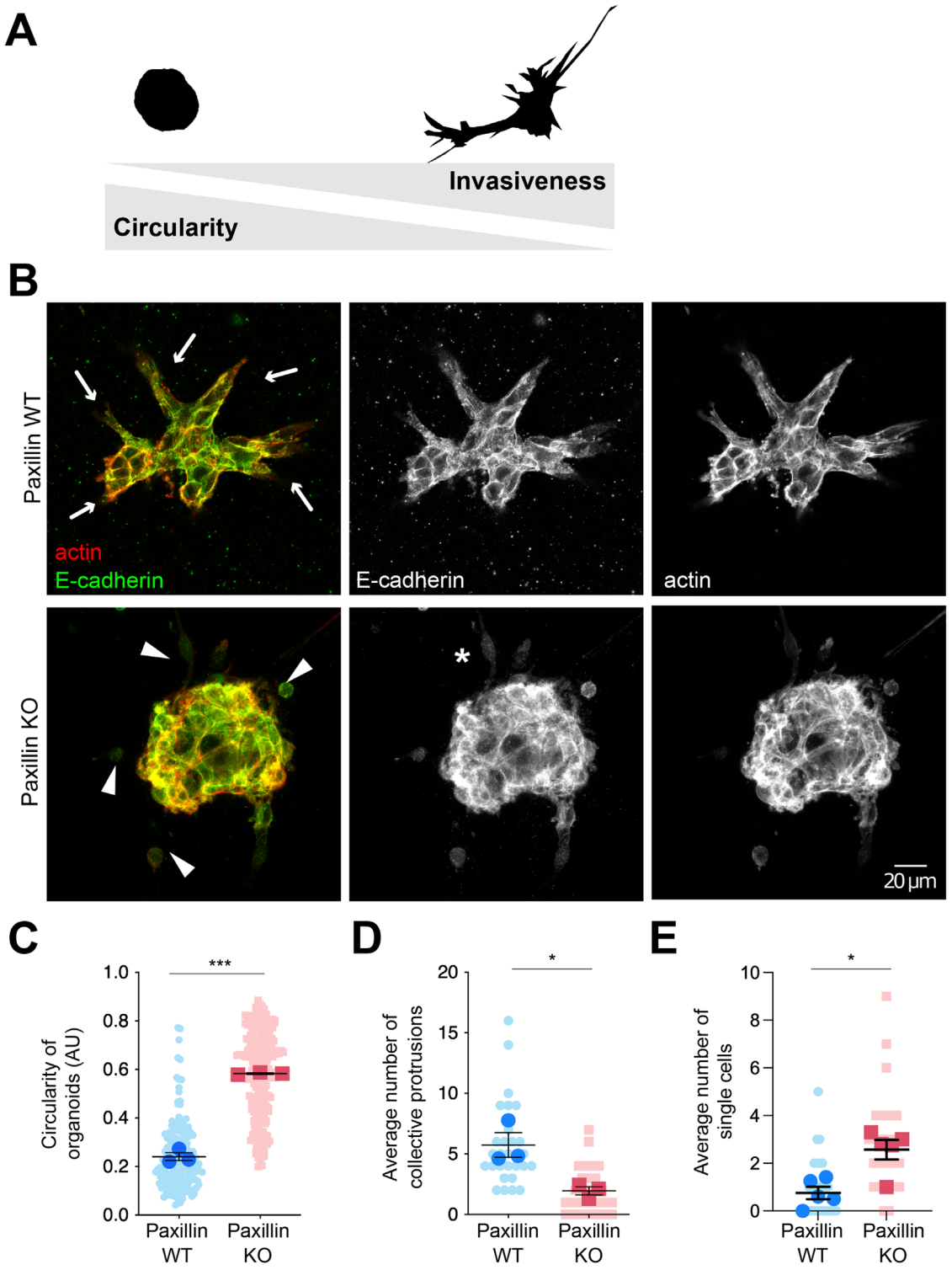

FIGURE 3: Paxillin KO tumor organoids are less invasive. (A) Illustration of the Fiji-generated masks of tumor organoids. A high degree of circularity of the organoid correlates with low invasiveness. (B) Representative confocal images of tumor organoids. Arrows point to collective cell protrusions in paxillin WT organoids; arrowheads point to individual tumor cells in paxillin KO organoids. The asterisk indicates a hyper mesenchymal cell in a paxillin KO organoid. (C) Quantification of organoid circularity. Three animals per genotype; *n* (paxillin WT) = 172 organoids, *n* (paxillin KO) = 215 organoids. (D) Quantification of the average number of collective protrusions per organoid; *n* = 3 animals per genotype. (E) Quantification of the average number of single cells per field; *n* = 5 animals per genotype. A Student's *t* test was performed for statistical analysis for C, D. A Mann–Whitney U test was performed for E. Data represent mean ± SEM *< 0.05, **< 0.01, ***< 0.001.

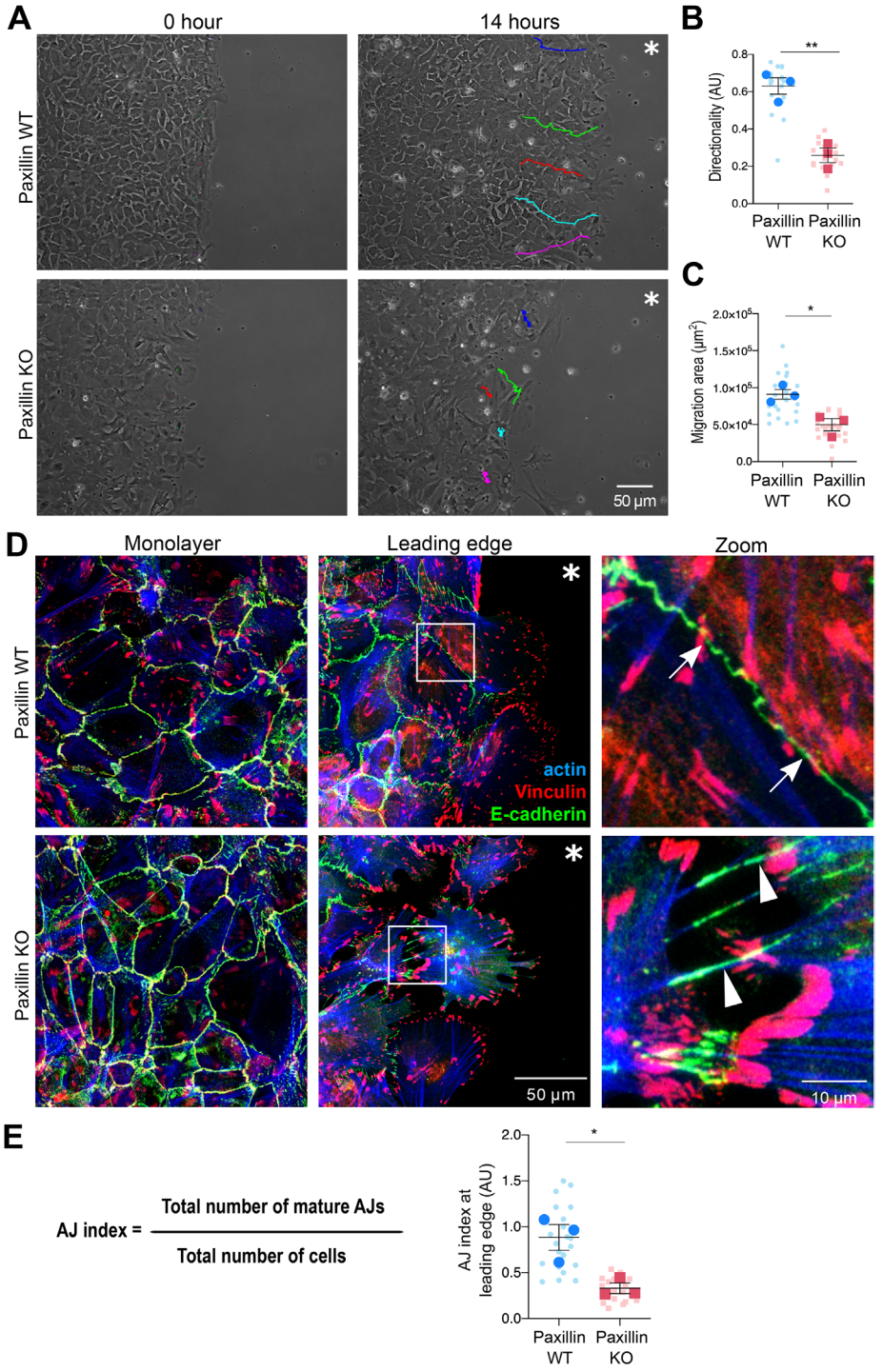

FIGURE 4: Paxillin KO tumor cells have defective collective migration on a 2D substrate. (A) Still images from phase-contrast movies of tumor cell migration for 14 h postwound. Colored lines indicate the tracks of individual cells at the wound edge from initial position (0 h) to final position (14 h). Asterisk indicates the wound area. (B) Directionality of cells at the wound edge; $n = 3$ animals per genotype. A minimum of five movies per animal, five cells per movie. (C) Area of cells migrated into the wound; $n = 3$ animals per genotype. A minimum of five movies per animal, five cells per movie. (D) Tumor cells stained for E-cadherin, vinculin, and F-actin after 8 h of migration. Representative images of AJs in the monolayer or at the leading edge. Arrows point to mature AJs; arrowheads point to disorganized AJs. Asterisk indicates the wound area. (E) AJ index was defined as the total number of mature AJs vs. the total number of cells at the wound edge; $n = 3$ animals per genotype. Each dot represents one image. A Student's *t* test was performed for statistical analysis. Data represent mean ± SEM *< 0.05, **< 0.01.

focal adhesions, were unable to efficiently reform AJs (Figure 5, A and B). Taken together, these data indicate that paxillin is necessary for both the stable maintenance of mature AJs and the formation of new AJs after their perturbation.

To determine if paxillin may be controlling AJ organization via regulation of E-cadherin trafficking (Brüser and Bogdan, 2017), we performed surface biotinylation assays to measure the endocytic rate of plasma membrane E-cadherin (Wagoner *et al.*, 2008). Paxillin WT and KO tumor cells were serum-starved and surface-labeled with biotin and then serum was reintroduced to induce E-cadherin endocytosis. While both WT and KO cells expressed similar levels of surface E-cadherin, the paxillin KO tumor cells exhibited a significantly reduced internalization rate of E-cadherin (Figure 5, C and E), suggesting that endocytic trafficking of AJ components is perturbed as compared with paxillin WT tumor cells.

In addition, we also assessed the recycling rates of E-cadherin in WT and KO tumor cells back to the cell surface (Wagoner *et al.*, 2008). In paxillin WT tumor cells, the surface E-cadherin level was only marginally changed during the first 30 min, which is potentially due to endocytic trafficking dominating the vesicle trafficking events. After 30 min, surface E-cadherin steadily increased over the next 60 min in the paxillin WT cells (Figure 5, D and F). However, in the paxillin KO cells, the level of E-cadherin at the plasma membrane remained relatively constant over time (Figure 5, D and F), suggesting that the recycling of E-cadherin as well as its endocytosis is perturbed in the absence of paxillin. Taken together, the data suggest that paxillin is an important contributor to maintaining the optimal E-cadherin turnover at the cell surface to facilitate AJ organization and integrity (Brüser and Bogdan, 2017).

Inhibition of HDAC6 activity partially rescues AJ organization and collective cell invasion in paxillin KO tumor cells

We have previously reported that paxillin inhibits HDAC6 activity to regulate MT (de) acetylation and control of apical protein recycling in the developing mouse mammary gland (Xu *et al.*, 2019). Additionally, paxillin depletion in mesenchymal cells results in disruption of anterograde vesicle trafficking in an HDAC6-dependent manner (Dubois *et al.*, 2017). Therefore we hypothesized that paxillin-dependent E-cadherin trafficking in tumor cells may also be regulated via HDAC6 inhibition. Accordingly, the 2D-cultured cell

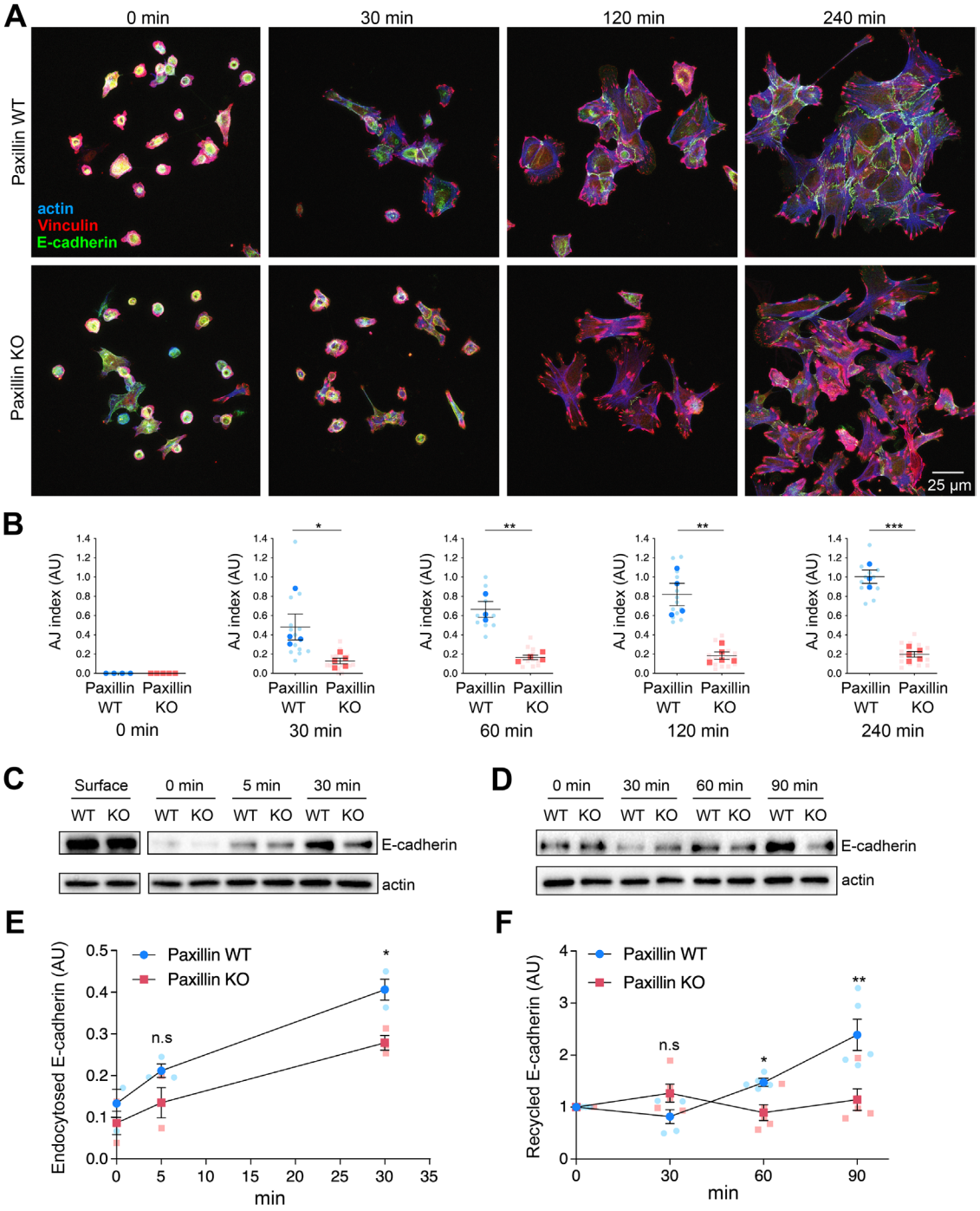

FIGURE 5: Paxillin is required for AJ formation involving endocytosis and recycling of junctional E-cadherin. (A) A calcium switch assay was used to monitor recovery of AJ integrity in cell islands. Cell AJ recovery was monitored following addition of calcium for time indicated. Cells were stained for E-cadherin, vinculin, and F-actin. (B) Quantification of the number of mature AJs per cell at indicated time points after calcium restoration; $n = 3$ animals per genotype. Each dot represents one image of a cell island. (C) Endocytosed biotin-labeled E-cadherin in paxillin WT or paxillin KO tumor cells during a calcium switch assay. (D) Biotin-labeled E-cadherin recycled to the cell surface during AJ formation during a calcium switch assay. (E) The internalized E-cadherin levels were normalized to total surface E-cadherin for each genotype; $n = 3$ animals per genotype. (F) Recycled E-cadherin to the cell surface at different time points was normalized to 0 min for each genotype; $n = 5$ animals per genotype. A Student's *t* test was performed for statistical analysis for B, E, and F; a Mann–Whitney U test was performed for B 30 min and E 5 min. Data represent mean ± SEM *< 0.05, **< 0.01, ***< 0.001.

colonies were treated with the HDAC6-specific inhibitor tubacin (Haggarty *et al.*, 2003). AJ organization was assessed by quantifying the percentage of mature AJs and disorganized AJs. In paxillin WT cells, both DMSO- and tubacin-treated cells exhibited 80% mature AJs (Figure 6, A and B), whereas tubacin treatment of the paxillin KO tumor cells increased the percentage of mature AJs (~55%) as

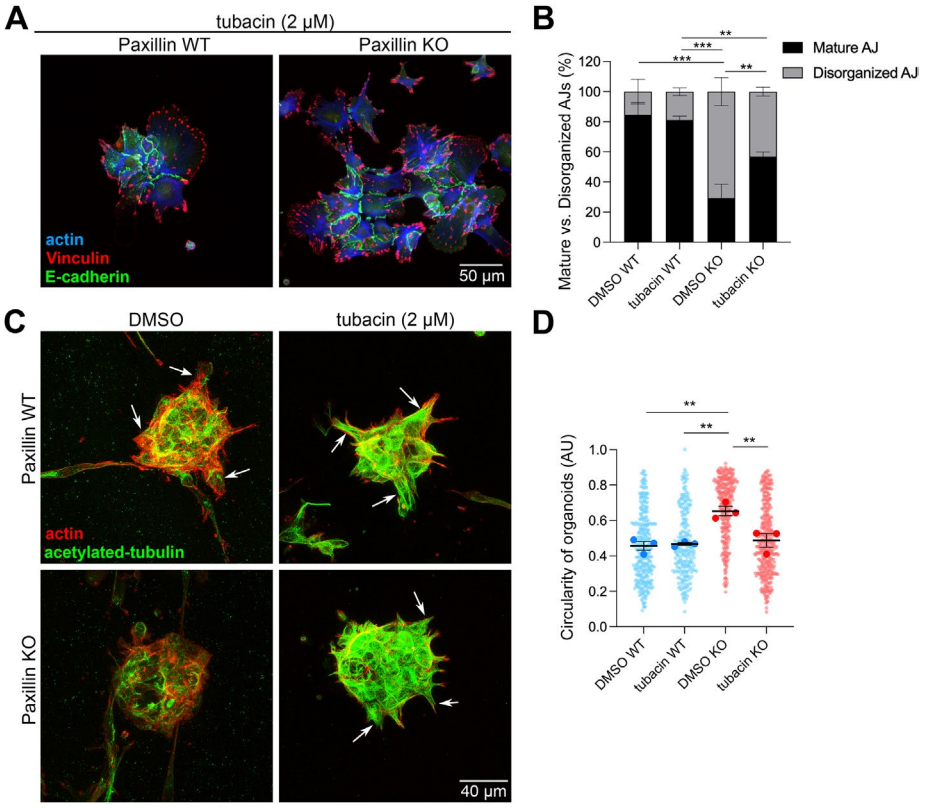

FIGURE 6: MT acetylation is important for AJ organization in tumor cell islands and for tumor organoid invasion. (A) Representative images of paxillin WT and paxillin KO tumor cells in 2D treated with tubacin (2 μM) and stained for E-cadherin, vinculin, and F-actin. (B) Quantification of the percentage of mature AJs and disorganized AJs; $n = 3$ animals per genotype. (C) Representative confocal images of 3D tumor organoids treated with DMSO or tubacin (2 μM). Both paxillin WT and paxillin KO organoids showed high levels of acetylated-tubulin after tubacin treatment. Tubacin-treated paxillin KO organoids showed increased collective cell invasion as compared with the DMSO-treated paxillin KO organoids. Arrows point to collective cell invasion. (D) Quantification of organoid circularity; $n = 3$ animals per genotype. Each dot represents one organoid. A one-way ANOVA analysis with Tukey's multiple comparison was performed for statistical analysis. Data represent mean ± SEM *< 0.05, **< 0.01, ***< 0.001.

compared with DMSO-treated KO cells (~30%) (Figure 6B). These data indicate that paxillin regulation of HDAC6 activity contributes in part to mature AJ organization.

Since we observed a decreased level of collective invasion in paxillin KO tumor organoids (Figure 3), we sought to examine whether tubacin treatment can also rescue this phenotype. Tumor organoids were subjected to a 2-day tubacin treatment and evaluated for their ability to form collective cell protrusions. The DMSO-treated paxillin KO tumor organoids exhibited a low level of invasion, combined with reduced acetylated-tubulin levels, as compared with DMSO-treated paxillin WT tumor organoids (Figure 6C and Supplemental Figure S7). Following tubacin treatment, the paxillin KO tumor organoids exhibited hyper-MT acetylation and a significant decrease in circularity, more indicative of increased invasiveness (Figures 3A and 6, C and D). Taken together, the data suggest that paxillin–HDAC6-regulated MT acetylation is important for collective tumor invasion.

Paxillin affects AJ integrity through balancing Rho GTPase activity

In addition to trafficking-dependent AJ organization, paxillin also plays a well-established role as a hub for the regulation of Rho family GTPase activity via cell–ECM signaling (Turner *et al.*, 1999; Turner, 2000; Deakin and Turner, 2011; Deakin *et al.*, 2012; López-Colomé *et al.*, 2017). Rho GTPase activity is also critical for AJ organization, with reduced Rac1 and elevated RhoA activity contributing to AJ maturation and maintenance (Braga *et al.*, 2000; Bruewer *et al.*, 2004; Acharya *et al.*, 2018; Braga, 2018; Gupta *et al.*, 2021). Additionally, during 2D collective migration, leader cells also generate cell–ECM traction forces via actomyosin-mediated contractility downstream of RhoA, thereby dragging the following cells (Friedl and Alexander, 2011; Haeger *et al.*, 2015). We therefore hypothesized that paxillin-dependent regulation of Rho GTPase activity may be required for mature AJ maintenance and collective cell movement.

Treatment of 2D-cultured paxillin WT tumor cells with the ROCK inhibitor Y27632, which blocks myosin-based contractility downstream of RhoA, or blebbistatin, which specifically inhibits myosin II activity, resulted in the loss of mature AJs and the emergence of more disorganized AJs (Figure 7A) (Uehata *et al.*, 1997), similar to those observed in the paxillin KO cells. Therefore RhoA and Rac1 GTPase activities were evaluated following a calcium switch assay. While no differences were observed at the earlier time points, at 60 min after the readdition of calcium, the paxillin KO cells exhibited a slightly elevated level of active Rac1 and a reduced level of active RhoA (Supplemental Figure S8). To determine if these perturbations in RhoGTPase activities may be contributing to the reduced formation of mature AJs in the paxillin KO cells, we treated them with the Rac1 inhibitor (NSC23766) or the RhoA activator (RhoA activator II) and quantified the percentage of mature versus disorganized AJs (Figure 7, B and D). Interestingly, the paxillin KO tumor cells, treated with the Rac1 inhibitor or RhoA activator, formed more mature AJs as compared with DMSO-treated paxillin KO cells (Figure 7B). Statistical analysis revealed that for the paxillin KO cells, the percentage of mature AJs was significantly rescued by these two drugs, while the increase in AJ index followed a similar trend but was not statistically significant (Figure 7, C and D).

To further characterize the role of paxillin in the regulation of RhoGTPase activity and function, we assessed the impact of these drug treatments on 2D migrating cells in the wound healing assay and evaluated the AJ formation in the cells at the wound edge (Figure 7E). Both blebbistatin and Y27632 caused AJ perturbation in the paxillin WT cells while the Rac1 inhibitor and RhoA activator partially rescued AJs in the paxillin KO tumor cells at the leading edge (Figure 7, F and G). Taken together, these results suggest that paxillin is important for AJ organization in tumor cells, partially through regulation of the balance of RhoA and Rac1 activity.

DISCUSSION

Paxillin has a well-established role in regulating single cell migration (Turner, 2000; Webb *et al.*, 2004; Deakin and Turner, 2008) and we

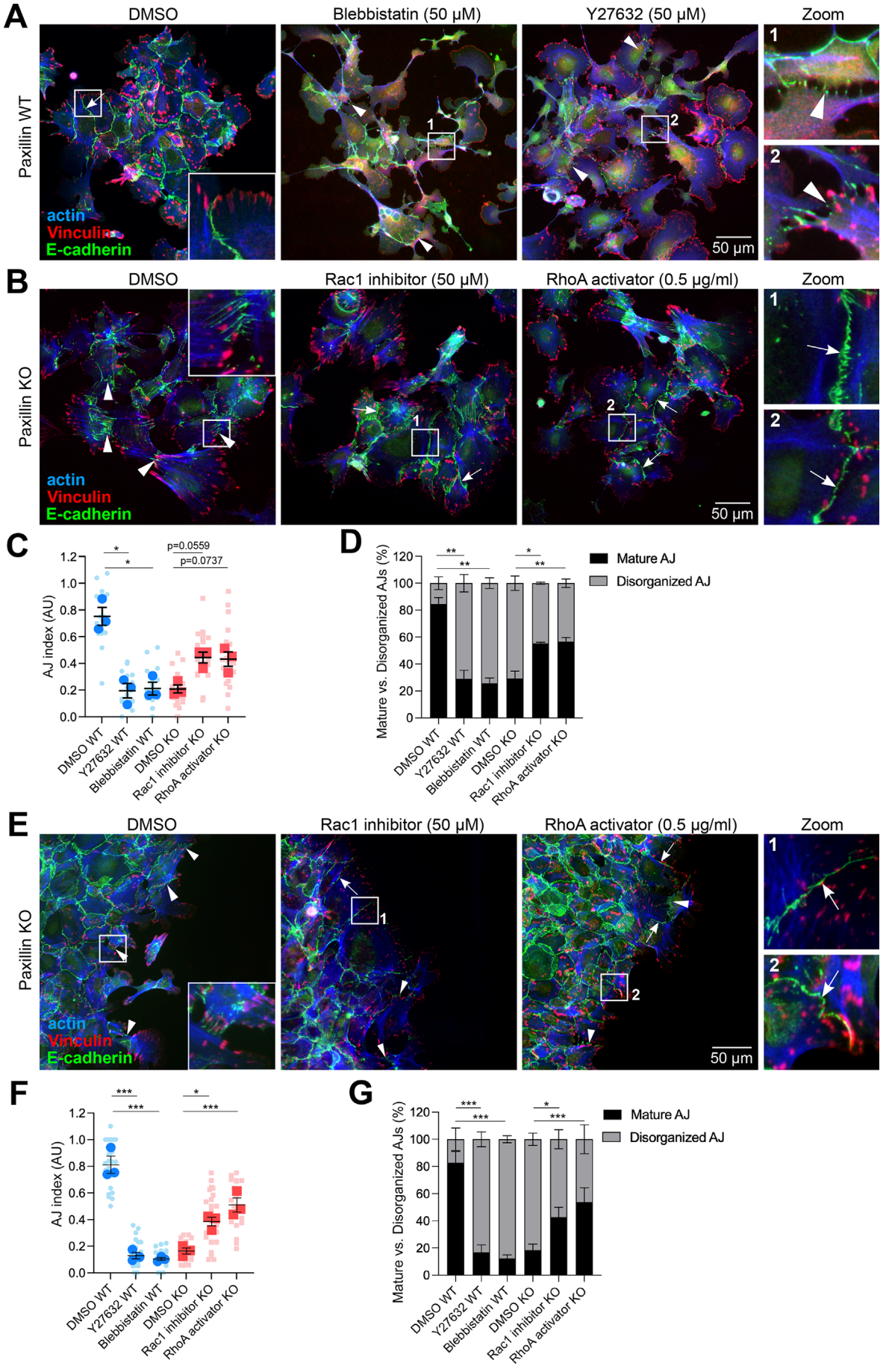
A
DMSO
Blebbistatin (50 μM)
Y27632 (50 μM)
Zoom
Paxillin WT
actin
Vinculin
E-cadherin
50 μm
B
DMSO
Rac1 inhibitor (50 μM)
RhoA activator (0.5 μg/ml)
Zoom
Paxillin KO
actin
Vinculin
E-cadherin
50 μm
C
AJ index (AU)
p=0.0559
p=0.0737
DMSO WT
Y27632 WT
Blebbistatin WT
DMSO KO
Rac1 inhibitor KO
RhoA activator KO
D
Mature vs. Disorganized AJs (%)
Mature AJ
Disorganized AJ
E
DMSO
Rac1 inhibitor (50 μM)
RhoA activator (0.5 μg/ml)
Zoom
Paxillin KO
actin
Vinculin
E-cadherin
50 μm
F
AJ index (AU)
G
Mature vs. Disorganized AJs (%)
Mature AJ
Disorganized AJ

previously showed that paxillin RNAi-treated individual MDA-MB-231 breast cancer cells have impaired migration in 3D ECMs and exhibit a reduction in surface lung metastases in an experimental metastasis mouse model (Deakin and Turner, 2011). However, paxillin's role in the early stages of tumor malignancy has not been evaluated. Herein, using a recently generated conditional paxillin KO mouse model (Rashid *et al.*, 2017; Xu *et al.*, 2019) crossed with the MMTV-PyMT spontaneous breast cancer mouse model, we identified critical roles for paxillin in facilitating breast cancer cell collective invasion and distant lung metastasis in vivo in part through a previously unappreciated paxillin-dependent regulation of cell–cell AJ integrity involving an E-cadherin endocytic/recycling pathway, paxillin-HDAC6-MT acetylation, and potentially a paxillin-Rho GTPase activity signaling axis.

The paxillin KO tumor mouse developed fewer lung metastases without any significant change of tumor size, latency, or cell proliferation (Figure 1 and Supplemental Figure S1). Interestingly, however, while the WT animals showed evidence of collective rather than single cell invasion, as previously observed in the PYMT model (Padmanaban *et al.*, 2019), the paxillin KO primary tumors failed to invade collectively into the surrounding stroma, with only a few single cells invading beyond the tumor edge (Figure 2). The long-established view of tumor malignancy is associated with increased EMT, as it provides a mechanism of escape for individual cancer cells in part due to the loss of AJs (Ye and Weinberg, 2015; Aiello *et al.*, 2018). However, more recent studies, including this report, have revealed that many tumors only undergo a partial EMT and tumor cells successfully metastasize to distant organs as collective cell populations (Zhao *et al.*, 2004; Rivenbark *et al.*, 2013). Indeed, clinical studies have revealed that in inflammatory breast cancer (Kleer *et al.*, 2001), invasive ductal carcinoma of the breast (Rodriguez *et al.*, 2012), and various other types of cancers (Sundfeldt *et al.*, 1997; Kim *et al.*, 2016), distant metastases originated from E-cadherin positive tumors that had only undergone a partial EMT. Furthermore, E-cadherin KO in the PyMT tumor mouse model, which promoted a shift from collective to single cell invasion, also resulted in reduced lung metastasis (Padmanaban *et al.*, 2019).

Tumor cell invasion involves complex cross-talk between the primary tumor cells and the cells and matrix components of the surrounding stroma (Friedl and Alexander, 2011; Haeger *et al.*, 2015; Ilina *et al.*, 2020). Using an ex vivo 3D organoid culture system, where the influence of the stroma is diminished, we confirmed that paxillin KO tumor organoids exhibited fewer collective cell protrusions, combined with a small increase in the number of invading single cells (Figure 3), indicating that paxillin is playing a cell autonomous role in regulating AJ maintenance to promote tumor invasiveness. Nevertheless, both cell–cell contacts and cell–ECM contacts contribute to collective cell invasion (Ilina *et al.*, 2020), and a recent study revealed that, mediated by the confinement of the surrounding connective tissue ECM, tumor cells collectively invade the stroma utilizing β1 and αVβ3/β5 integrins to form an invasive niche with highly aligned matrices (Haeger *et al.*, 2020). Furthermore, functional blockage of β1 integrins disrupted collective invasion and induced single cell dissemination (Hegerfeldt *et al.*, 2002), likely involving the activation of FAK, Src, and integrin-linked kinase downstream of classical ECM-integrin signaling (Monferran *et al.*, 2008; Eke *et al.*, 2012). Although we did not observe any significant change in phospho- or total FAK levels in the KO tumor cells versus the WT cells (Supplemental Figure S9), paxillin, which functions primarily as an adapter/scaffold protein at focal adhesion sites (Turner, 2000), was enriched along with vinculin at the tips of WT tumor leader cells (Supplemental Figure S3B) where it likely contributes to integrin-dependent signaling and subsequent cross-talk with AJs (Zegers *et al.*, 2003; Deakin *et al.*, 2012; Bays *et al.*, 2014; Bays and DeMali, 2017; Ladoux and Mège, 2017).

In addition to controlling 3D organoid tumor collective invasion, we showed that paxillin is also required for 2D collective tumor cell migration during wound repair involving the maintenance of mature E-cadherin-based AJs, as opposed to the more disorganized AJs, which predominate in the paxillin KO cells at the wound edge (Figure 4). Similar defects in AJ organization and integrity were observed during AJ recovery from calcium depletion (Figure 5). Interestingly, the AJs in the center of the 2D-cultured paxillin KO tumor monolayers remained mostly unperturbed (Figure 4D), as was observed in the primary tumor (Figure 2G). We speculate that this is due to tissue confinement, which is controlled by cell density (Abercrombie and Heaysman, 1953; Stoker and Rubin, 1967), cell shape (Bi *et al.*, 2015), cellular forces (Schötz *et al.*, 2013), and the physics of cell–cell contacts (Garcia *et al.*, 2015). Only when the cells begin to move into the surrounding stroma or wound do AJs become more dynamic (Nalbant *et al.*, 2009; Indra *et al.*, 2018) and the paxillin KO cells fail to maintain their cell–cell contacts.

How paxillin, which does not localize to AJs (Turner *et al.*, 1991), mediates AJ stability appears to involve several interdependent cellular processes and signaling pathways. First, using the calcium switch assay, we showed that paxillin KO cells exhibited impaired E-cadherin endocytosis and recycling (Figure 5, C–F). In both physiologic (tissue development) and pathologic (wound repair or tumor invasion) situations, AJs have been shown to be highly dynamic structures that remodel rapidly (Friedl and Gilmour, 2009; Yonemura, 2011; Brüser and Bogdan, 2017). Importantly, paxillin has been shown to promote anterograde vesicle trafficking to the plasma membrane (Dubois *et al.*, 2017) via paxillin binding to and inhibition of HDAC6 and thereby regulation of MT (de)acetylation (Deakin and Turner, 2014; Dubois *et al.*, 2017). Similarly, during normal mammary gland development, paxillin facilitates ductal morphogenesis and apical-basal polarity formation through regulation of MT acetylation and a Rab11/MyoVb-dependent trafficking

FIGURE 7: Paxillin maintains AJs in part through regulation of Rho GTPase activity. (A) Paxillin WT cells were treated with Myosin II inhibitor blebbistatin (50 μM) or ROCK inhibitor Y27632 (50 μM) for 4 h and then stained for the AJ markers E-cadherin, vinculin, and F-actin. Arrowheads point to disorganized AJs. (B) Paxillin KO cells were treated with Rac1 inhibitor NSC23766 (50 μM) or RhoA activator RhoA activator II (0.5 μg/ml) for 4 h and then stained for E-cadherin, vinculin, and F-actin. Arrows point to mature AJs; arrowheads point to disorganized AJs. (C) Quantification of AJ index; $n = 3$ animals per genotype. Each dot represents one image. (D) Quantification of the percentage of mature AJs and disorganized AJs; $n = 3$ animals per genotype. (E) Representative images of paxillin KO tumor cells from migration assays for 8 h with DMSO, NSC23766, or RhoA activator II treatment. Arrows point to mature AJs; arrowheads point to disorganized AJs. (F) Quantification of AJ index of cells at the leading wound edge for paxillin WT or paxillin KO cells treated with drugs as indicated; $n = 3$ animals per genotype. Each dot represents one image. (G) Quantification of the percentage of mature AJs and bridge AJs; $n = 3$ animals per genotype. Statistical analysis was performed using a one-way ANOVA analysis with Tukey's multiple comparison. Data represent mean ± SEM *< 0.05, **< 0.01, ***< 0.001.

mechanism (Xu *et al.*, 2019). Interestingly, the paxillin WT tumor organoids also have a higher level of acetylated MTs as compared with the paxillin KO tumor organoids (Supplemental Figure S7) and tubacin treatment, which inhibits HDAC6-mediated MT deacetylation activity (Haggarty *et al.*, 2003), partially rescued collective invasion in the paxillin KO 3D tumor organoids, as well as AJ maturation in 2D-cultured paxillin KO tumor cells (Figure 6). We speculate that paxillin may control E-cadherin vesicle trafficking through MT acetylation-dependent recruitment and function of MT-associated motor proteins (Reed *et al.*, 2006).

Paxillin regulation of Rho GTPase activity was also found to be involved in AJ organization, with the KO cells exhibiting modestly reduced RhoA and elevated Rac1 activity during junction recovery following calcium depletion (Figure 7 and Supplemental Figure S8). AJs are intimately associated with the F-actin cytoskeleton and transmit forces between cells via RhoA-mediated actomyosin contractility (Friedl and Gilmour, 2009; Yonemura, 2011; Acharya *et al.*, 2018; Gupta *et al.*, 2021). At mature AJs, pulling and pushing forces generated by different population of actin filaments (branched or bundled) reach a dynamic balance (Efimova and Svitkina, 2018; Heuzé *et al.*, 2019). However, when the force balance is impaired, AJs become destabilized, leaving gaps between the cell–cell interface, thus promoting the formation of less stable AJs (Heuzé *et al.*, 2019) (Figure 4, E and F).

In mesenchymal cells, paxillin localizes to and regulates the turnover rate of focal adhesions, in part through mediating the localized recruitment of Rac1 and RhoA regulators and their effectors such as β-PIX, Vav2, and the p21-activated kinase (PAK) (Turner *et al.*, 1999; Tsubouchi *et al.*, 2002; Jones *et al.*, 2013) to drive the remodeling of the actin cytoskeleton and promote cell migration (Tsubouchi *et al.*, 2002; Brown and Turner, 2004; Deakin and Turner, 2008; Deakin *et al.*, 2012). However, since paxillin does not localize to AJs (Turner *et al.*, 1991), the mechanism by which it controls Rho GTPase signaling to regulate AJ organization is likely to be indirect, involving its recruitment to cell–ECM adhesions in the tumor leader cells (Supplemental Figure S3B). Importantly, several of paxillin's binding partners, including vinculin, β-PIX, and PAK, are enriched at both cell-matrix adhesions and AJs (Zegers *et al.*, 2003; Deakin and Turner, 2008; Deakin *et al.*, 2012; Bays *et al.*, 2014; Bays and DeMali, 2017; Ladoux and Mège, 2017) and are therefore potential candidates for mediating this cross-talk between the two locations. Additionally, paxillin, through its regulation of MT acetylation and stability, could potentially control GEFH1-MT binding to regulate its activity (Krendel *et al.*, 2002), which in turn controls Rac1 or RhoA signaling at the cell's leading edge (Nalbant *et al.*, 2009), and has also been shown to regulate localized RhoA activity at cell–cell junctions (Nalbant *et al.*, 2009; Hatte *et al.*, 2018).

In summary, our study demonstrates an unexpected role for paxillin in breast tumor invasion and metastasis through the regulation of tumor cell collective movement, in part via controlling the integrity of cell–cell of AJs. Future studies will focus on understanding how paxillin is able to coordinate and integrate E-cadherin trafficking and the spatio-temporal activity of Rho GTPase family members to optimize AJ functionality.

MATERIALS AND METHODS

Request a protocol through *Bio-protocol*.

Animals

All mouse experiments were performed in compliance with protocols approved by SUNY Upstate Medical University IACUC. The paxillin$^{fl/fl}$MMTV-cre mice were generated as previously described (Xu *et al.*, 2019) and the paxillin$^{fl/fl}$ mouse line has been deposited at the Jackson Laboratories (Bar Harbor, ME). Paxillin$^{fl/+}$cre mice were then bred with MMTV-PyMT mice (obtained from Jackson Labs) and maintained on a mixed genetic background (C57BL/6J and FVB/N). The paxillin$^{+/+}$crePyMT mouse is abbreviated as wild-type (WT) mouse and the paxillin$^{fl/fl}$crePyMT mouse is abbreviated as knockout (KO) mouse.

Antibodies and reagents

Antibodies used were rabbit polyclonal anti-paxillin (H114) (Santa Cruz Biotechnology) (1:100 for immunostaining, 1:1000 for Western blotting), mouse anti-E-cadherin (1:100) (610182; BD Biosciences), rabbit anti-E-cadherin (1:100) (3195; Cell Signaling), mouse anti-p120 Catenin (1:100) (610134; BD Biosciences), rat anti-EpCAM (1:100) (Developmental Studies Hybridoma Bank, University of Iowa), and mouse anti-Rac1 (1:1000) (610650; BD Biosciences). Rhodamine-phalloidin (1:500) (R415; Cat# PHDR1, Cytoskeleton, Denver, CO) was used to visualize F-actin; DAPI (D9542; Sigma-Aldrich, St. Louis, MO) was used to visualize nuclei. Secondary antibodies used were DyLight 488–conjugated goat anti-mouse (1:250) (35502; Thermo Fisher) DyLight 550–conjugated goat anti-mouse (1:250) (84540; Thermo Fisher), DyLight 488–conjugated goat anti-rabbit (1:250) (35552; Thermo Fisher), DyLight 550–conjugated goat anti-rabbit (1:250) (84541; Thermo Fisher), and Alexa Fluor 488 AffiniPure goat anti-rat (1:250) (112-545-003; Jackson ImmunoResearch).

Inhibitors and activators

Rac1 inhibitor (NSC23766) (50 μM) (MilliporeSigma, Burlington, MA), RhoA activator II (0.5 μg/ml) (Cat# CN03, Cytoskeleton), HDAC6 inhibitor tubacin (2 μM) (SML0065; MilliporeSigma), ROCK inhibitor Y-27632 (50 μM) (10005584; Cayman), or blebbistatin (50 μM) (B0560 MilliporeSigma) were used for the times indicated.

Histology

Primary tumors were washed with phosphate-buffered saline (PBS), fixed in 4% paraformaldehyde (PFA) for 4 h at room temperature, perfused in 30% sucrose solution overnight at 4°C, embedded in TissueTek optimal cutting temperature (OCT) compound (Sakura USA), and cryosectioned (6 μm) as previously described (Goreczny *et al.*, 2017). Tumor sections were subjected to standard H&E staining or immunofluorescence staining. A Zeiss Axioskop2 plus microscope fitted with a QImaging EXi Blue charge-coupled device camera and Plan-Apochromat 10× or 20× objective was used to image tumor sections.

Tumor latency and growth analysis

Female mice carrying the PyMT transgene were palpated weekly after tumor onset. To measure the tumor volume, the long and short axes of tumors were measured using digital calipers. Individual tumor volume was calculated using the equation volume (mm^3) = (short axis^2) × (long axis/2).

Results for both the total tumor burden (sum of all tumor volumes per mouse) (Figure 1A) and primary tumor volume (Supplemental Figure S1A) are displayed.

In vivo metastasis quantification

Lungs were evaluated when primary tumors reached 2 cm. Lungs were fixed in 4% PFA in PBS and then embedded in OCT. Ten-micron cryosections were collected every 250 μm and stained using standard H&E. The total number of metastases on each section was summed to determine the total number of lung metastasis.

Multicell versus single cell invasion quantification

EpCAM or E-cadherin staining of tumor sections was used for quantifying multicell versus single cell invasion into the stroma. Each string or group of tumor cells within the stroma was scored as a multicell invasion event. Each single tumor cell observed in the stroma was counted as a single cell invasion event.

Immunofluorescence microscopy

Cells on FN-coated glass coverslips were fixed with 4% PFA in PBS for 15 min, permeabilized with 1% Triton X-100 in PBS for 15 min, quenched with 0.1 M glycine for 15 min, and blocked with 3% bovine serum albumin (BSA) for 1 h at room temperature. Coverslips were then incubated with primary antibodies as indicated, diluted in 3% BSA for 2 h at 37°C, followed by 1 h incubation in secondary antibodies. F-actin was stained with rhodamine-phalloidin (Cat# PHDR1, Cytoskeleton, Denver, CO) and nuclei were stained with DAPI (Sigma-Aldrich, St. Louis, MO). Cells were imaged using a Leica SP8 laser scanning confocal microscope and a HPX Plan Apochromat 63× /1.4 NA oil λ BL objective or a Zeiss Axioskop2 plus microscope, fitted with a Q imagin ExiBlue charge-coupled device camera using an Apochromat 20× objective.

Immunoblotting

Samples of the bulk tumor, which contain both tumor cells and stromal cells, or isolated primary tumor cells, were lysed in SDS–PAGE sample buffer, electrophoresed through 10% SDS polyacrylamide gels, and transferred to nitrocellulose (Life Science). The membranes were blocked with 3% BSA for 30 min and probed with primary and secondary antibodies and then visualized and quantified by chemiluminescence (SuperSignal West; Thermo Fisher Scientific) using a Chemidoc MP imaging system (Bio-Rad).

3D tumor organoid invasion

The 3D tumor organoids were prepared as previously described (Nguyen-Ngoc *et al.*, 2015). Briefly, tumors were minced and shaken for 60 min at 37°C in digestion media (2 mg/ml collagenase [C2139; Sigma Aldrich], 2 mg/ml trypsin [85450C; Sigma], 5 µg/ml insulin [I9278; Sigma], 5% vol/vol fetal bovine serum [FBS], and 1% vol/vol penicillin/streptomycin in DMEM/F12). The dissociated tumor cell suspension was centrifuged at 400 × *g* for 10 min followed by incubation with 80 U of DNase (D4263; Sigma). Four rounds of differential centrifugation at 400 × *g* for 5 s were performed to separate the stroma cells from tumor cells. The pelleted tumor cells were either directly plated onto collagen gels or frozen in liquid nitrogen.

Tumor organoid invasion assays were performed in 24-well tissue culture plates. Fifty:50 ddH_2O:Bovine collagen I (Purecol, Advanced Biomatrix, San Diego, CA) was mixed with 1/10th the volume of 10× minimum essential media (MEM) and titrated to pH 7.2–7.6 using 0.1 M NaOH. Aliquots (400 µl) of the collagen gel solution were added to each well and allowed to solidify for 3–4 h at 37°C. Tumor organoids were suspended in culture media (DMEM/F12, 10% vol/vol FBS, 2 mM L-glutamine, and 1% vol/vol penicillin/streptomycin) at a density of 1000 organoids/ml, seeded on the top of the solidified collagen gels, and cultured for the indicated length of the time. The tumor organoid invasion index was quantified after 4 d from seeding. Invasiveness was scored by measuring the circularity of an organoid using the Analyze particles plugin in ImageJ/Fiji.

2D cell migration assay

Glass coverslips were coated with 10 µg/ml FN in PBS for 1 h at 37°C, then overlayed with silicon cell chambers (80209; ibidi US, Fitchburg, Wisconsin). Primary tumor cells were isolated as above and plated on culture dishes for spreading overnight. A total concentration of 2×10^5 cell/ml primary tumor cells was then seeded into the silicon chambers and cultured overnight to form a cell monolayer. After 16 h, the silicon chambers were removed. Cells were briefly washed with PBS and supplemented with complete culture media or drug-containing media for migration. For immunofluorescence analyses, cells were fixed after 8 h of migration. For live cell analyses, cells were tracked using a Nikon TE2000 inverted microscope equipped with a temperature/CO_2-regulated environmental chamber. Images were acquired with a 20× objective lens at 10-min intervals for 14 h. The Manual tracking plugin in ImageJ was used to track the cell centroid over the length of the movie. The Chemotaxis and Migration plugin in ImageJ was used to calculate directionality.

Calcium switch assay

Tumor cells were plated on 10 µg/ml FN-coated 2D substrates in complete culture media (DMEM/F12, 10% vol/vol FBS, 2 mM L-glutamine, and 1% vol/vol penicillin/streptomycin). After 16 h of culture at 37°C, cells were washed with PBS and treated with serum free, 2 mM EGTA DMEM/F12 for 2 h to induce calcium chelation and AJ disassembly. The EGTA media was then replaced with calcium-containing complete culture media to promote junction reassembly. For immunofluorescence analyses, cells were fixed at 0 and 30 min and 1, 2, and 4 h from recovery. For live cell analyses, cells were tracked using a Nikon TE2000 inverted microscope equipped with a temperature/CO_2-regulated environmental chamber, and images were acquired with 10×/0.45 NA objective lens or 20× S Plan Fluor ELWD objective lens at 5-min intervals for 6 h.

Biotinylation assay for E-cadherin endocytosis

Isolated tumor cells ($0.5–1 \times 10^5$ cell/ml) were plated on 35-mm cell culture dishes for 2 d. Cells were starved in serum free media for 1 h at 37°C and then labeled with 1 mg/ml Sulfo-NHS-Biotin (Cat#21217, ThermoFisher) in PBS at 4°C for 1 h, followed by washing to remove free biotin. One plate of cells from each genotype was lysed directly in the plate with RIPA buffer (200 mM Tris-HCl, 150 mM NaCl, 1% TX-100, 0.1% SDS, 0.1% Sodium deoxycholate, 5 mM EDTA) after this step to obtain the total level of surface biotin-labeled E-cadherin. The other cells were then incubated in normal media for 0, 5, or 30 min at 37°C to allow for endocytosis to proceed. At the indicated times, the remaining cell surface biotin-labeling was removed using two, 20-min washes of 3.75 mg/ml sodium 2-mercaptoethanesulfonate (Cat#BCBC6477V, Sigma) solution at 4°C, followed by three washes in cold PBS. Next, cells were lysed in 300–400 µl of RIPA buffer. For the biotin-labeled protein pull down and the input control lysates, 10 µl of each lysate was subjected to Precision Red Advanced Protein Assay (ADV02, cytoskeleton, Inc.) to obtain the protein concentrations, 10 µl of each lysate was saved for input level, and the remainder of the biotin-labeled lysate was precipitated using 40 µl of streptavidin beads. The beads were washed three times in RIPA buffer and then boiled for 10 min in SDS–PAGE sample buffer. The surface and endocytosed E-cadherin were analyzed by immunoblotting.

Biotinylation assay for E-cadherin recycling

E-cadherin endocytosis was induced by replacing the culture media with 2 mM EGTA, and E-cadherin recycling to the plasma membrane was achieved by the readdition of calcium (Wagoner *et al.*, 2008). Isolated tumor cells were cultured for 2 d and then treated with 2 mM EGTA in serum free media for 2 h. After calcium depletion, cells were washed with PBS twice and allowed to recover in

normal calcium-containing media for 0, 30, 60, or 90 min. At the time points indicated, cells were washed with cold PBS twice on ice and then incubated with 1 mg/ml Sulfo-NHS-Biotin in PBS for 1 h at 4°C followed by washing in cold PBS three times to remove free biotin. Cells were lysed, and E-cadherin was harvested by streptavidin bead pull down and analyzed as described in the endocytosis assay.

Imaris analysis

Image analysis of cell area and aspect ratio were performed using Imaris x64 version 9.7.1 (Bitplane) and Prism 9. Cell membrane staining was used to manually segment individual cells into surfaces with the Imaris Surface Module. The cell area was calculated by taking the product of the number of voxels of each cell surface and the dimensions of the voxel.

$$\text{Area of surface } (\mu m^2) = (\text{number of voxels}) \times (\text{Dimension of voxel})$$

The cell aspect ratio was quantitated by taking the ratio of the median (minor for a 2D surface) and the longest (major) principal diameter of the object-oriented bounding box.

Active Rac1 pull-down assay

Active Rac1 pull-down assays were performed using PAK-PBD beads (PAK02; Cytoskeleton, Denver, CO). Briefly, cells were lysed in RIPA buffer (50 mM Tris-HCl, 150 mM NaCl, 1% Triton X-100, 0.5% Na-deoxycholate, 0.1% SDS, 1 mM EDTA, and protease inhibitor cocktail) for 15 min on ice. Lysates were centrifuged at 18,000 rpm for 10 min, and the supernatants were collected. Twenty micrograms of GST-PAK-PBD beads were washed three times using RIPA buffer. Cell lysates (600–800 µg) were incubated with the beads at 4°C for 4 h. After incubation, the beads were washed three times using wash buffer (25 mM Tris pH 7.5, 30 mM MgCl2, and 40 mM NaCl). SDS–PAGE sample buffer was added to suspend the beads and boiled for 10 min at 100°C. Active Rac1 was then detected by Western blot by using mouse anti-Rac1 (1:1000, 610650; BD Biosciences) and normalized to the actin level in the total lysate (mouse clone C4, 1:2000, MAB1501, MilliporeSigma).

G-LISA RhoA activation assay

Active RhoA was detected following the manufactory's instructions (BK036; Cytoskeleton, Denver, CO). Briefly, cells were washed with cold PBS and lysed in ice-cold lysis buffer. Protein concentration was adjusted to 0.4 mg/ml. After adding an equal volume of binding buffer, assays were performed using 1.2 µg of protein per well. Samples were shaken on ice for 30 min at a speed of 200 rpm and then washed three times with washing buffer. Antigen-presenting buffer was added for 2 min before removal; samples were then incubated with anti-RhoA primary antibody (1:250) at room temperature for 45 min, washed three times, and incubated with secondary antibody (1:62.5) for another 45 min. HRP detection reagent was added, and absorbance was measured at 490 nm with an Emax Precision Microplate Reader (Molecular Devices, Sunnyvale, CA).

Statistical analysis

A Shapiro–Wilk test was performed for the normality analysis. A two-sided Student's *t* test was performed if the dataset passed the normality test; otherwise, a Mann–Whitney test was performed for comparison between two experimental groups. One-way ANOVA analysis with a Tukey's multiple comparison was performed to compare three or more groups. Datasets were generated from at least three independent animals per genotype. Statistical significance is indicated by $^*P < 0.05$, $^{**}P < 0.01$, $^{***}P < 0.001$. Data are mean ± SEM.

ACKNOWLEDGMENTS

We thank the members of the Turner lab for insightful discussions and Elizabeth Luke and Theresa Stowell for expert technical assistance. This work was supported by the National Institutes of Health (R35 GM131709) and the Carol Baldwin Breast Cancer Research Fund of Central New York to C.E.T.

REFERENCE

Abercrombie M, Heaysman JE (1953). Observations on the social behaviour of cells in tissue culture. I. Speed of movement of chick heart fibroblasts in relation to their mutual contacts. Exp Cell Res 5, 111–131.

Acharya BR, Nestor-Bergmann A, Liang X, Gupta S, Duszyc K, Gauquelin E, Gomez GA, Budnar S, Marcq P, Jensen OE, *et al.* (2018). A Mechanosensitive RhoA pathway that protects epithelia against acute tensile stress. Dev Cell 47, 439–452.e436.

Aiello NM, Maddipati R, Norgard RJ, Balli D, Li J, Yuan S, Yamazoe T, Black T, Sahmoud A, Furth EE, *et al.* (2018). EMT subtype influences epithelial plasticity and mode of cell migration. Dev Cell 45, 681–695.e684.

Alpha KM, Xu W, Turner CE (2020). Paxillin family of focal adhesion adaptor proteins and regulation of cancer cell invasion. Int Rev Cell Mol Biol 355, 1–52.

Azuma K, Tanaka M, Uekita T, Inoue S, Yokota J, Ouchi Y, Sakai R (2005). Tyrosine phosphorylation of paxillin affects the metastatic potential of human osteosarcoma. Oncogene 24, 4754–4764.

Bays JL, DeMali KA (2017). Vinculin in cell–cell and cell-matrix adhesions. Cell Mol Life Sci 74, 2999–3009.

Bays JL, Peng X, Tolbert CE, Guilluy C, Angell AE, Pan Y, Superfine R, Burridge K, DeMali KA (2014). Vinculin phosphorylation differentially regulates mechanotransduction at cell–cell and cell-matrix adhesions. J Cell Biol 205, 251–263.

Bhattacharjee A, Richards WG, Staunton J, Li C, Monti S, Vasa P, Ladd C, Beheshti J, Bueno R, Gillette M, *et al.* (2001). Classification of human lung carcinomas by mRNA expression profiling reveals distinct adenocarcinoma subclasses. Proc Natl Acad Sci USA 98, 13790–13795.

Bi D, Lopez JH, Schwarz JM, Manning ML (2015). A density-independent rigidity transition in biological tissues. Nat Phys 11, 1074–1079.

Bonnans C, Chou J, Werb Z (2014). Remodelling the extracellular matrix in development and disease. Nat Rev Mol Cell Biol 15, 786–801.

Braga V (2018). Signaling by small GTPases at cell–cell junctions: Protein interactions building control and networks. Cold Spring Harbor Perspectives Biology 10, a028746.

Braga VM, Betson M, Li X, Lamarche-Vane N (2000). Activation of the small GTPase Rac is sufficient to disrupt cadherin-dependent cell–cell adhesion in normal human keratinocytes. Mol Biol Cell 11, 3703–3721.

Brown MC, Turner CE (2004). Paxillin: adapting to change. Physiol Rev 84, 1315–1339.

Brown MC, West KA, Turner CE (2002). Paxillin-dependent paxillin kinase linker and p21-activated kinase localization to focal adhesions involves a multistep activation pathway. Mol Biol Cell 13, 1550–1565.

Bruewer M, Hopkins AM, Hobert ME, Nusrat A, Madara JL (2004). RhoA, Rac1, and Cdc42 exert distinct effects on epithelial barrier via selective structural and biochemical modulation of junctional proteins and F-actin. Am J Physiol Cell Physiol 287, C327–C335.

Brüser L, Bogdan S. (2017). Adherens junctions on the move—membrane trafficking of E-cadherin. Cold Spring Harb Perspect Biol 9, a029140.

Cai D, Chen SC, Prasad M, He L, Wang X, Choesmel-Cadamuro V, Sawyer JK, Danuser G, Montell DJ (2014). Mechanical feedback through E-cadherin promotes direction sensing during collective cell migration. Cell 157, 1146–1159.

Carthew RW (2005). Adhesion proteins and the control of cell shape. Curr Opin Genet Dev 15, 358–363.

Cheung KJ, Ewald AJ (2016). A collective route to metastasis: Seeding by tumor cell clusters. Science 352, 167–169.

Cheung KJ, Gabrielson E, Werb Z, Ewald AJ (2013). Collective invasion in breast cancer requires a conserved basal epithelial program. Cell 155, 1639–1651.

De Palma M, Biziato D, Petrova TV (2017). Microenvironmental regulation of tumour angiogenesis. Nat Rev Cancer 17, 457–474.

Deakin NO, Ballestrem C, Turner CE (2012). Paxillin and Hic-5 interaction with vinculin is differentially regulated by Rac1 and RhoA. PLoS One 7, e37990.

Deakin NO, Turner CE (2008). Paxillin comes of age. J Cell Sci 121, 2435–2444.

Deakin NO, Turner CE (2011). Distinct roles for paxillin and Hic-5 in regulating breast cancer cell morphology, invasion, and metastasis. Mol Biol Cell 22, 327–341.
Deakin NO, Turner CE (2014). Paxillin inhibits HDAC6 to regulate microtubule acetylation, Golgi structure, and polarized migration. J Cell Biol 206, 395–413.
Dillekås H, Rogers MS, Straume O (2019). Are 90% of deaths from cancer caused by metastases? Cancer Med 8, 5574–5576.
Dubois F, Alpha K, Turner CE (2017). Paxillin regulates cell polarization and anterograde vesicle trafficking during cell migration. Mol Biol Cell 28, 3815–3831.
Efimova N, Svitkina TM (2018). Branched actin networks push against each other at adherens junctions to maintain cell–cell adhesion. J Cell Biol 217, 1827–1845.
Eke I, Deuse Y, Hehlgans S, Gurtner K, Krause M, Baumann M, Shevchenko A, Sandfort V, Cordes N (2012). β Integrin/FAK/cortactin signaling is essential for human head and neck cancer resistance to radiotherapy. J Clin Invest 122, 1529–1540.
Farmer P, Bonnefoi H, Becette V, Tubiana-Hulin M, Fumoleau P, Larsimont D, Macgrogan G, Bergh J, Cameron D, Goldstein D, *et al.* (2005). Identification of molecular apocrine breast tumours by microarray analysis. Oncogene 24, 4660–4671.
Farooqui R, Fenteany G (2005). Multiple rows of cells behind an epithelial wound edge extend cryptic lamellipodia to collectively drive cell-sheet movement. J Cell Sci 118, 51–63.
Friedl P, Alexander S. (2011). Cancer invasion and the microenvironment: Plasticity and reciprocity. Cell 147, 992–1009.
Friedl P, Borgmann S, Bröcker EB (2001). Amoeboid leukocyte crawling through extracellular matrix: lessons from the Dictyostelium paradigm of cell movement. J Leukoc Biol 70, 491–509.
Friedl P, Gilmour D (2009). Collective cell migration in morphogenesis, regeneration and cancer. Nat Rev Mol Cell Biol 10, 445–457.
Friedl P, Wolf K (2008). Tube travel: the role of proteases in individual and collective cancer cell invasion. Cancer Res 68, 7247–7249.
Garcia S, Hannezo E, Elgeti J, Joanny JF, Silberzan P, Gov NS (2015). Physics of active jamming during collective cellular motion in a monolayer. Proc Natl Acad Sci USA 112, 15314–15319.
George M, Bullo F, Campàs O (2017). Connecting individual to collective cell migration. Sci Rep 7, 9720.
Ginsburg O, Bray F, Coleman MP, Vanderpuye V, Eniu A, Kotha SR, Sarker M, Huong TT, Allemani C, Dvaladze A, *et al.* (2017). The global burden of women's cancers: a grand challenge in global health. Lancet 389, 847–860.
Goreczny GJ, Ouderkirk-Pecone JL, Olson EC, Krendel M, Turner CE (2017). Hic-5 remodeling of the stromal matrix promotes breast tumor progression. Oncogene 36, 2693–2703.
Greaves S (2000). Zipping up adhesion. Nat Cell Biol 2, E45–E45.
Greig J, Bulgakova NA (2020). Interplay between actomyosin and E-cadherin dynamics regulates cell shape in the Drosophila embryonic epidermis. J Cell Sci 133, jcs.242321.
Gupta S, Duszyc K, Verma S, Budnar S, Liang X, Gomez GA, Marcq P, Noordstra I, Yap AS (2021). Enhanced RhoA signaling stabilizes E-cadherin in migrating epithelial monolayers. J Cell Sci 134, JCS258767.
Haeger A, Alexander S, Vullings M, Kaiser FMP, Veelken C, Flucke U, Koehl GE, Hirschberg M, Flentje M, Hoffman RM, *et al.* (2020). Collective cancer invasion forms an integrin-dependent radioresistant niche. J Exp Med 217, e20181184.
Haeger A, Wolf K, Zegers MM, Friedl P (2015). Collective cell migration: guidance principles and hierarchies. Trends Cell Biol 25, 556–566.
Haggarty SJ, Koeller KM, Wong JC, Grozinger CM, Schreiber SL (2003). Domain-selective small-molecule inhibitor of histone deacetylase 6 (HDAC6)-mediated tubulin deacetylation. Proc Natl Acad Sci USA 100, 4389–4394.
Hamidi H, Ivaska J (2018). Every step of the way: integrins in cancer progression and metastasis. Nat Rev Cancer 18, 533–548.
Hatte G, Prigent C, Tassan JP (2018). Tight junction-associated protein GEF-H1 in the neighbours of dividing epithelial cells is essential for adaptation of cell–cell membrane during cytokinesis. Exp Cell Res 371, 72–82.
Hegerfeldt Y, Tusch M, Bröcker EB, Friedl P (2002). Collective cell movement in primary melanoma explants: plasticity of cell–cell interaction, beta1-integrin function, and migration strategies. Cancer Res 62, 2125–2130.
Heuzé ML, Sankara Narayana GHN, D'Alessandro J, Cellerin V, Dang T, Williams DS, Van Hest JC, Marcq P, Mège RM, Ladoux B (2019). Myosin II isoforms play distinct roles in adherens junction biogenesis. Elife 8, e46599.
Ilina O, Campanello L, Gritsenko PG, Vullings M, Wang C, Bult P, Losert W, Friedl P (2018). Intravital microscopy of collective invasion plasticity in breast cancer. Dis Model Mech 11, dmm034330.
Ilina O, Gritsenko PG, Syga S, Lippoldt J, La Porta CAM, Chepizhko O, Grosser S, Vullings M, Bakker GJ, Starruss J, *et al.* (2020). Cell–cell adhesion and 3D matrix confinement determine jamming transitions in breast cancer invasion. Nat Cell Biol 22, 1103–1115.
Indra I, Choi J, Chen C-S, Troyanovsky RB, Shapiro L, Honig B, Troyanovsky SM (2018). Spatial and temporal organization of cadherin in punctate adherens junctions. Proc Natl Acad Sci USA 115, E4406–E4415.
Iyer KV, Piscitello-Gómez R, Paijmans J, Jülicher F, Eaton S (2019). Epithelial viscoelasticity is regulated by mechanosensitive E-cadherin turnover. Curr Biol 29, 578–591.e575.
Jones MC, Machida K, Mayer BJ, Turner CE (2013). Paxillin kinase linker (PKL) regulates Vav2 signaling during cell spreading and migration. Mol Biol Cell 24, 1882–1894.
Kametani Y, Takeichi M (2007). Basal-to-apical cadherin flow at cell junctions. Nat Cell Biol 9, 92–98.
Kanteti R, Yala S, Ferguson MK, Salgia R (2009). MET, HGF, EGFR, and PXN gene copy number in lung cancer using DNA extracts from FFPE archival samples and prognostic significance. J Environ Pathol Toxicol Oncol 28, 89–98.
Keely PJ (2011). Mechanisms by which the extracellular matrix and integrin signaling act to regulate the switch between tumor suppression and tumor promotion. J Mammary Gland Biol Neoplasia 16, 205–219.
Kim SA, Inamura K, Yamauchi M, Nishihara R, Mima K, Sukawa Y, Li T, Yasunari M, Morikawa T, Fitzgerald KC, *et al.* (2016). Loss of CDH1 (E-cadherin) expression is associated with infiltrative tumour growth and lymph node metastasis. Br J Cancer 114, 199–206.
Kleer CG, van Golen KL, Braun T, Merajver SD (2001). Persistent E-cadherin expression in inflammatory breast cancer. Mod Pathol 14, 458–464.
Krendel M, Zenke FT, Bokoch GM (2002). Nucleotide exchange factor GEF-H1 mediates cross-talk between microtubules and the actin cytoskeleton. Nat Cell Biology 4, 294–301.
Ladoux B, Mège RM (2017). Mechanobiology of collective cell behaviours. Nat Rev Mol Cell Biol 18, 743–757.
LaLonde DP, Grubinger M, Lamarche-Vane N, Turner CE (2006). CdGAP associates with actopaxin to regulate integrin-dependent changes in cell morphology and motility. Curr Biol 16, 1375–1385.
Lambert AW, Pattabiraman DR, Weinberg RA (2017). Emerging biological principles of metastasis. Cell 168, 670–691.
Le TL, Yap AS, Stow JL (1999). Recycling of E-cadherin: a potential mechanism for regulating cadherin dynamics. J Cell Biol 146, 219–232.
Lichtner RB, Julian JA, North SM, Glasser SR, Nicolson GL (1991). Coexpression of cytokeratins characteristic for myoepithelial and luminal cell lineages in rat 13762NF mammary adenocarcinoma tumors and their spontaneous metastases. Cancer Res 51, 5943–5950.
Lin EY, Jones JG, Li P, Zhu L, Whitney KD, Muller WJ, Pollard JW (2003). Progression to malignancy in the polyoma middle t oncoprotein mouse breast cancer model provides a reliable model for human diseases. Am J Pathol 163, 2113–2126.
López-Colomé AM, Lee-Rivera I, Benavides-Hidalgo R, López E (2017). Paxillin: a crossroad in pathological cell migration. J Hematol Oncol 10, 50.
Monferran S, Skuli N, Delmas C, Favre G, Bonnet J, Cohen-Jonathan-Moyal E, Toulas C (2008). Alphavbeta3 and alphavbeta5 integrins control glioma cell response to ionising radiation through ILK and RhoB. Int J Cancer 123, 357–364.
Nalbant P, Chang Y-C, Birkenfeld J, Chang Z-F, Bokoch GM (2009). Guanine nucleotide exchange factor-H1 regulates cell migration via localized activation of RhoA at the leading edge. Mol Biol Cell 20, 4070–4082.
Nguyen-Ngoc KV, Shamir ER, Huebner RJ, Beck JN, Cheung KJ, Ewald AJ (2015). 3D culture assays of murine mammary branching morphogenesis and epithelial invasion. Methods Mol Biol 1189, 135–162.
Nobes CD, Hall A (1999). Rho GTPases control polarity, protrusion, and adhesion during cell movement. J Cell Biol 144, 1235–1244.
Obenauf AC, Massagué J (2015). Surviving at a distance: organ-specific metastasis. Trends Cancer 1, 76–91.
Padmanaban V, Krol I, Suhail Y, Szczerba BM, Aceto N, Bader JS, Ewald AJ (2019). E-cadherin is required for metastasis in multiple models of breast cancer. Nature 573, 439–444.
Padmanaban V, Tsehay Y, Cheung KJ, Ewald AJ, Bader JS (2020). Between-tumor and within-tumor heterogeneity in invasive potential. PLoS Comput Biol 16, e1007464–e1007464.
Panková K, Rösel D, Novotný M, Brábek J (2010). The molecular mechanisms of transition between mesenchymal and amoeboid invasiveness in tumor cells. Cell Mol Life Sci 67, 63–71.

Paterson AD, Parton RG, Ferguson C, Stow JL, Yap AS (2003). Characterization of E-cadherin endocytosis in isolated MCF-7 and chinese hamster ovary cells: the initial fate of unbound E-cadherin. J Biol Chem 278, 21050–21057.
Pinheiro D, Bellaiche Y (2018). Mechanical force-driven adherens junction remodeling and epithelial dynamics. Dev Cell 47, 3–19.
Quail DF, Joyce JA (2013). Microenvironmental regulation of tumor progression and metastasis. Nat Med 19, 1423–1437.
Radvanyi L, Singh-Sandhu D, Gallichan S, Lovitt C, Pedyczak A, Mallo G, Gish K, Kwok K, Hanna W, Zubovits J, *et al.* (2005). The gene associated with trichorhinophalangeal syndrome in humans is overexpressed in breast cancer. Proc Natl Acad Sci USA 102, 11005–11010.
Rashid M, Belmont J, Carpenter D, Turner CE, Olson EC (2017). Neural-specific deletion of the focal adhesion adaptor protein paxillin slows migration speed and delays cortical layer formation. Development 144, 4002–4014.
Reed NA, Cai D, Blasius TL, Jih GT, Meyhofer E, Gaertig J, Verhey KJ (2006). Microtubule acetylation promotes kinesin-1 binding and transport. Curr Biol 16, 2166–2172.
Rivenbark AG, O'Connor SM, Coleman WB (2013). Molecular and cellular heterogeneity in breast cancer: challenges for personalized medicine. Am J Pathol 183, 1113–1124.
Rodriguez FJ, Lewis-Tuffin LJ, Anastasiadis PZ (2012). E-cadherin's dark side: possible role in tumor progression. Biochim Biophys Acta 1826, 23–31.
Schaller MD (2001). Paxillin: a focal adhesion-associated adaptor protein. Oncogene 20, 6459–6472.
Scheswohl DM, Harrell JR, Rajfur Z, Gao G, Campbell SL, Schaller MD (2008). Multiple paxillin binding sites regulate FAK function. J Mol Signal 3, 1.
Schötz EM, Lanio M, Talbot JA, Manning ML (2013). Glassy dynamics in three-dimensional embryonic tissues. J R Soc Interface 10, 20130726.
Short SM, Yoder BJ, Tarr SM, Prescott NL, Laniauskas S, Coleman KA, Downs-Kelly E, Pettay JD, Choueiri TK, Crowe JP, *et al.* (2007). The expression of the cytoskeletal focal adhesion protein paxillin in breast cancer correlates with HER2 overexpression and may help predict response to chemotherapy: a retrospective immunohistochemical study. Breast J 13, 130–139.
Stebbing J, Delaney G, Thompson A (2007). Breast cancer (non-metastatic). BMJ Clin Evid 2007, 0102.
Stoker MG, Rubin H (1967). Density dependent inhibition of cell growth in culture. Nature 215, 171–172.
Stoletov K, Kato H, Zardouzian E, Kelber J, Yang J, Shattil S, Klemke R (2010). Visualizing extravasation dynamics of metastatic tumor cells. J Cell Sci 123, 2332–2341.
Sundfeldt K, Piontkewitz Y, Ivarsson K, Nilsson O, Hellberg P, Brännström M, Janson PO, Enerback S, Hedin L (1997). E-cadherin expression in human epithelial ovarian cancer and normal ovary. Int J Cancer 74, 275–280.
Takahashi I, Onodera K, Sasano Y, Mizoguchi I, Bae JW, Mitani H, Kagayama M, Mitani H (2003). Effect of stretching on gene expression of beta1 integrin and focal adhesion kinase and on chondrogenesis through cell-extracellular matrix interactions. Eur J Cell Biol 82, 182–192.
Thuroff F, Goychuk A, Reiter M, Frey E (2019). Bridging the gap between single cell migration and collective dynamics. Elife 8, e46842.
Tsubouchi A, Sakakura J, Yagi R, Mazaki Y, Schaefer E, Yano H, Sabe H (2002). Localized suppression of RhoA activity by Tyr31/118-phosphorylated paxillin in cell adhesion and migration. J Cell Biol 159, 673–683.
Turashvili G, Bouchal J, Baumforth K, Wei W, Dziechciarkova M, Ehrmann J, Klein J, Fridman E, Skarda J, Srovnal J, *et al.* (2007). Novel markers for differentiation of lobular and ductal invasive breast carcinomas by laser microdissection and microarray analysis. BMC Cancer 7, 55.
Turner CE (2000). Paxillin and focal adhesion signalling. Nat Cell Biol 2, E231–E236.
Turner CE, Brown MC, Perrotta JA, Riedy MC, Nikolopoulos SN, McDonald AR, Bagrodia S, Thomas S, Leventhal PS (1999). Paxillin LD4 motif binds PAK and PIX through a novel 95-kD ankyrin repeat, ARF-GAP protein: A role in cytoskeletal remodeling. J Cell Biol 145, 851–863.
Turner CE, Glenney JR Jr, Burridge K (1990). Paxillin: a new vinculin-binding protein present in focal adhesions. J Cell Biol 111, 1059–1068.
Turner CE, Kramarcy N, Sealock R, Burridge K (1991). Localization of paxillin, a focal adhesion protein, to smooth muscle dense plaques, and the myotendinous and neuromuscular junctions of skeletal muscle. Exp Cell Res 192, 651–655.
Uehata M, Ishizaki T, Satoh H, Ono T, Kawahara T, Morishita T, Tamakawa H, Yamagami K, Inui J, Maekawa M, *et al.* (1997). Calcium sensitization of smooth muscle mediated by a Rho-associated protein kinase in hypertension. Nature 389, 990–994.
Vadlamudi R, Adam L, Tseng B, Costa L, Kumar R (1999). Transcriptional up-regulation of paxillin expression by heregulin in human breast cancer cells. Cancer Research 59, 2843–2846.
van Zijl F, Krupitza G, Mikulits W (2011). Initial steps of metastasis: cell invasion and endothelial transmigration. Mutat Res 728, 23–34.
Vitorino P, Meyer T (2008). Modular control of endothelial sheet migration. Genes Dev 22, 3268–3281.
Wagoner MP, Ling K, Anderson RA (2008). Tracking the transport of E-cadherin to and from the plasma membrane. Methods Mol Biol 457, 267–278.
Webb DJ, Donais K, Whitmore LA, Thomas SM, Turner CE, Parsons JT, Horwitz AF (2004). FAK-Src signalling through paxillin, ERK and MLCK regulates adhesion disassembly. Nat Cell Biol 6, 154–161.
Xu W, Gulvady AC, Goreczny GJ, Olson EC, Turner CE (2019). Paxillin-dependent regulation of apical-basal polarity in mammary gland morphogenesis. Development 146, dev174367.
Yamada S, Nelson WJ (2007). Localized zones of Rho and Rac activities drive initiation and expansion of epithelial cell–cell adhesion. J Cell Biol 178, 517–527.
Yang HJ, Chen JZ, Zhang WL, Ding YQ (2010). Focal adhesion plaque associated cytoskeletons are involved in the invasion and metastasis of human colorectal carcinoma. Cancer Invest 28, 127–134.
Yates LR, Knappskog S, Wedge D, Farmery JHR, Gonzalez S, Martincorena I, Alexandrov LB, Van Loo P, Haugland HK, Lilleng PK, *et al.* (2017). Genomic evolution of breast cancer metastasis and relapse. Cancer Cell 32, 169–184.e167.
Ye X, Weinberg RA (2015). Epithelial-mesenchymal plasticity: a central regulator of cancer progression. Trends Cell Biol 25, 675–686.
Yonemura S (2011). Cadherin-actin interactions at adherens junctions. Curr Opin Cell Biol 23, 515–522.
Zegers MM, Forget MA, Chernoff J, Mostov KE, ter Beest MB, Hansen SH (2003). Pak1 and PIX regulate contact inhibition during epithelial wound healing. EMBO j 22, 4155–4165.
Zhao H, Langerød A, Ji Y, Nowels KW, Nesland JM, Tibshirani R, Bukholm IK, Kåresen R, Botstein D, Børresen-Dale AL, *et al.* (2004). Different gene expression patterns in invasive lobular and ductal carcinomas of the breast. Mol Biol Cell 15, 2523–2536.